JOURNAL OF GEOPHYSICAL RESEARCH, VOL. 106, NO. D14, PAGES 14,989–15,014, JULY 27, 2001

An overview of microphysical properties of Arctic clouds observed in May and July 1998 during FIRE ACE

R. Paul Lawson, Brad A. Baker, and Carl G. Schmitt
SPEC Incorporated, Boulder, Colorado

T. L. Jensen
Silver Lining Enterprises, Fort Collins, Colorado

Abstract. Microphysical data were collected by the NCAR C-130 research aircraft during the First International Satellite Cloud Climatology Project (ISCCP) Regional Experiment Arctic Cloud Experiment (FIRE ACE). Boundary layer clouds 100 to 400 m thick were observed on 11 of the 16 missions. The all-water clouds varied from being adiabatic and homogeneous with monomodal drop spectra to subadiabatic and inhomogeneous with bimodal drop spectra and drizzle. The subadiabatic clouds were observed to be actively mixing near cloud top. The adiabatic clouds provided a test of the performance of the liquid water content (LWC) probes but only in low LWC conditions. A mixed-phase boundary layer cloud displayed striking variability in the hydrometeor fields on a horizontal scale of 10 km and a vertical scale of 100 m. Cloud Particle Imager (CPI) data showed separate regions with small supercooled cloud drops, supercooled drizzle (at -25°C) and graupel particles. A deep stratus cloud with its base at 2 km (+2°C) and top at 6 km (-25°C) contained drizzle near cloud top and (lower in the cloud) very high (2500 to 4000 L^{-1}) concentrations of ice particles in conditions that did not meet all the Hallett-Mossop criteria. CPI data showed that an Arctic cirrus cloud was composed of very high (~100,000 L^{-1}) concentrations of small ice particles interspersed with single, large (mostly bullet rosette) crystals. The data showed that the cirrus cloud was inhomogeneous on scales down to tens of meters. The average ice particle concentrations measured in the cirrus by the FSSP and CPI probes were several hundred to a few thousand per liter, much higher than commonly found in the literature.

1. Introduction

Cloud-radiative processes in the Arctic have a strong impact on the stability of the Arctic Ocean ice pack [*Curry et al.*, 1993] and also have ramifications on the global energy budget [e.g., *Intergovernmental Panel on Climate Change (IPCC)*, 1990]. Clouds in the boundary layer are persistent during May through September and strongly influence the melting rate of the pack ice [*Curry et al.*, 1996]. The cloudy boundary layer in the Arctic is low, optically thin, and increases the summertime melt rate of sea ice, since the long-wave exceeds the shortwave cloud-radiative forcing at the surface. A positive feedback scenario occurs as melt ponds and leads form, and the surface albedo decreases.

Prior to the 1997-1998 Surface HEat Budget of the Arctic (SHEBA) project [*Perovich et al.*, 1999] and the First ISCCP (International Satellite Cloud Climatology Project) Regional Experiment Arctic Clouds Experiment (FIRE ACE) [*Curry et al.*, 2000], there were relatively few aircraft studies of Arctic clouds. While many types of Arctic stratus clouds were investigated during SHEBA, including clouds with multiple layers that extended to above 500 mbar and cirrus, thin stratus clouds within 1 km of the surface occurred most frequently and were the clouds most often investigated by the in situ research aircraft. We focus our analysis in this paper on these clouds and refer to them as "cloudy layers" (after the terminology used by *Curry et al.* [1988, 1996], or "boundary layer clouds" (which was the terminology used by scientists at the FIRE ACE field project and used by *Curry et al.* [2000]). While Arctic boundary layer clouds may not always be thermodynamically or mechanically linked to the underlying surface, as is conventionally assumed in the classic definition, the term has been adopted here to represent low stratus cloud layers in the Arctic.

In addition to investigations of boundary layer clouds, microphysical measurements from a deep stratus cloud that extended from 2 km to 6 km are presented, as well as data from a cirrus cloud. These data are included to provide a better representation of the variability that exists in the many types of clouds observed in the Arctic. Also, the microphysical properties revealed in these investigations could be used to validate remote measurements and process models.

Curry et al. [1996] summarize findings from previous investigations of summertime Arctic cloudy boundary layers. The salient features from their study that relate to this research are summarized here.

1. Three types of summertime cloud boundary layers are identified: (1) a stable boundary layer with thin, patchy stable clouds that may be found in multiple layers, (2) a stable boundary layer, often with fog at the surface, which is topped by a cloud-topped mixed layer, and (3) a cloud-topped, well-mixed boundary layer that extends to the surface.

Paper number 2000JD900789.
0148-0227/01/2000JD900789$09.00

2. Warm, moist air flows from continental regions over the pack ice, and condensation is induced initially by radiative and diffusional cooling to the colder surface and longwave radiation to space.

3. Clouds in the boundary layer are often well mixed, with the mixing assumed to proceed downward from cloud top due to radiational cooling and overturning. The well-mixed layer may extend to the surface, in which case, surface effects may have also contributed to cloud formation.

4. The microphysical properties of clouds associated with the Arctic boundary layer are varied and definitive trends are difficult to establish. This may be due to the relatively small microphysical data set due to a lack of measurements. Significant ice concentrations are generally observed at temperatures colder than -15° to -20°C [*Jayaweera and Ohtake*, 1973; *Curry et al.*, 1990]. However, exceptions to this generality have been reported. Some ice has been observed in clouds at temperatures as warm as -4°C. A predominantly water cloud was observed (in wintertime) at a temperature of -32°C [*Witte*, 1968], and *Curry et al.* [1997] report an all-ice cloud at -14°C. Mixed-phase clouds are often observed, and the types of ice particles have not been well documented, except for surface-based observations. *Curry* [1986] found a significant amount of drizzle associated with a large dispersion in the droplet spectra.

The microphysical properties of FIRE ACE clouds are investigated here using data collected by the National Center for Atmospheric Research (NCAR) C-130 research aircraft during May and July 1998. The study includes, for the first time in the Arctic, a new particle imaging probe that provides high-definition digital images of cloud particles. Data from the Cloud Particle Imager (CPI) are analyzed to separate water drops from ice particles and identify crystal habits and to compute water and ice particle size distributions. The CPI is described in more detail, along with other microphysical instrumentation used in this study, in section 3.

The data presented in this paper are organized in the following way: A table gives an overview of the major physical features of clouds observed during the 16 C-130 missions in FIRE ACE, focusing on clouds associated with the boundary layer. An example of a boundary layer cloud, which is mostly adiabatic and homogeneous with a monomodal drop size distribution, is discussed. Measurements of cloud liquid water content (LWC) are compared with the theoretical adiabatic values in the boundary layer clouds that are identified as being adiabatic. An example of a boundary layer cloud that is nonadiabatic, actively mixing at cloud top, and inhomogeneous with bimodal drop size distribution is presented. Time series measurements of cloud LWC, droplet concentration, temperature, and vertical velocity at different levels in six boundary layer clouds are discussed. An example of a boundary layer cloud with highly variable hydrometeor fields is discussed in some detail. Images of particles and ice/water particle size distributions in a deep stratus cloud extending from 2 km to 6 km are presented. Lastly, an example of the inhomogeneous ("clumpy") distribution of particles in a cirrus cloud is discussed.

2. FIRE ACE Field Project

Curry et al., [2000] describe the SHEBA/FIRE ACE project in detail. Some salient features of the project which are pertinent to the C-130 flights are excerpted here. The main goal of the experiment was to examine the effects of clouds on radiation exchange among the surface, atmosphere, and space and to study how the surface influences the evolution of the cloudy boundary layer. Data collected during the field phase of the project are being used to evaluate and improve climate model parameterizations of Arctic cloud and radiation processes, satellite remote sensing of cloud and surface characteristics, and understanding of cloud-radiation feedbacks in the Arctic.

The location and timing of the FIRE Arctic Clouds Experiment were determined by the scheduled operations of the SHEBA experimental site in the Beaufort Sea during October 1997 to October 1998. The Canadian Coast Guard icebreaker *Des Groseilliers* was deployed in a multiyear ice floe on October 1, 1997, at 75°16.3'N, 142°41.2'W. The C-130 flights were planned to coincide with the current location of the ship as it drifted with the ice floe. Horizontal traverses of 20-200 km were made by the NCAR C-130 at various levels above, below, and within cloud, in the boundary layer, and at various altitudes to map the surface using aircraft remote sensing instruments. Additionally, slow ascents and descents were made to obtain high-resolution slant profiles using in situ instruments. The ferry flight from Fairbanks to the location of the *Des Groseilliers* generally took about 2 hours in each direction during May and nearly 3 hours in June, leaving 2 - 4 hours of on-station data collection.

3. Instrumentation

The capabilities of the NCAR C-130 and instrumentation on the research aircraft are described by *Curry et al.* [2000]. Of particular interest to this study are microphysical instruments used to measure cloud particle characteristics and cloud liquid water content (LWC), including (1) two King hot-wire LWC devices [*King et al.*, 1978] manufactured by Particle Measuring Systems with modifications to the electronics by NCAR, (2) a Gerber Scientific particulate volume monitor (PVM-100A) described by *Gerber et al.*, [1994], (3) a Particle Measuring Systems (PMS) Forward Scattering Spectrometer Probe (FSSP-100), described by *Knollenberg* [1981], (4) a PMS 260X one-dimensional optical array probe with 64 photo diodes at 10 μm pixel resolution, [*Knollenberg*, 1981], (5) very limited use of the shadow-or concentration from the PMS 2D-C two-dimensional optical array probe [*Knollenberg*, 1981], and (6) a CPI described briefly by *Lawson et al.* [1998], *Korolev et al.* [1999], and in more detail by *Lawson* [1997] and *Lawson and Jensen* [1998]. Table 1 shows a comparison of the sample volumes of the FSSP, 260X, 2D-C and CPI probes.

The King probe is a hot-wire device with airflow characteristics that are theoretically predictable. The response of the probe has been shown to rolloff for drops larger than about 50 μm [*Biter et al.*, 1987]. The King probes are mounted near each wingtip and close to the leading edge of the wing itself. Studies of the airflow around the probe installation on the C-130 have not been conducted. *Laursen* [1998] points out that the location close to the wing leading edge was a matter for concern, and one King probe was relocated and extended from the wing for one mission. However, Laursen reports that this appeared to make no discernable difference in the measurements. The King dry-air term is a function of the (local) true airspeed, and the dry-air term is subtracted from the in-cloud reading to obtain LWC.

Table 1. Sample Volumes (at 100 m s^{-1}) for Particle Probes Used in This Study

Probe	Sample Volume
FSSP	0.053 L/s
2D-C	5.1 L/s (maximum)
260X	4.9 L/s (maximum)
CPI PDS	0.470 L/s
CPI image	0.006 L/s (maximum)

2D-C, 260X, and CPI are shown as maximums because the depth of field is less than the dimension of the physical constraints of the sample volume for small particles. The sample volume for small (<~150 μm) particles is reduced by up to about a factor of ~50 for the 2D-C and by up to about a factor of 100 for the 260X and CPI.

It is therefore important to know the correct true airspeed at the probe location, or to subtract the dry-air term measured outside of cloud at the same airspeed and air density. In this study, the King probe data were used as supplied by NCAR; the dry-air term is computed assuming the airspeed at the probe location is the same as that measured by the aircraft data system. Magnitudes of the errors that may be induced as a result of neglecting airflow considerations are undetermined.

The PVM-100A is an optical device that measures LWC, drop surface area and effective radius at a sample rate of 1 KHz. The light scattered in the forward direction by an ensemble of drops is optically weighted and summed on a photodetector. The measurements presented here were averaged to 1 Hz by the NCAR data processing routine. The probe was initially supplied with an improper calibration, which was modified after the field experiment by Gerber Scientific Incorporated. The recalibrated data have been used in this paper.

Icing tunnel tests were conducted after the field experiment to calibrate the LWC devices. The King probes performed well in the tunnel after the gain of one of the probes was adjusted in software to compensate for an improper hardware setting. When the drop median volume diameter (MVD) was <~25 μm, both King probes generally measured LWC to within 10% of the tunnel value (J. W. Strapp, personal communication, 2000). The Gerber PVM probe on the C-130 was not functioning for the icing tunnel tests. The University of Washington (UW) operated an identical PVM probe during FIRE ACE, and its performance in the icing tunnel tests is discussed by *Garrett and Hobbs* [1999]. They report that during the small droplet tests the PVM underestimated LWC by 12% in the zero to 0.75 g m^{-3} range. An analysis of the response of the UW PVM-100A to large droplet sizes showed that it had diminished response to droplets with diameter larger than 20 μm. At an MVD of 32 μm the PVM underestimated spray LWC by ~40% (compared to the 18% underestimation at a MVD of 30 μm reported by *Gerber et al.* [1994]).

The FSSP has been under considerable scrutiny since its introduction into the field. Processing of FSSP data by NCAR for this project included partial recovery of losses due to coincidences and probe dead time [*Baumgardner et al.*, 1985], and adjustment of channel widths to account for airspeed corrections to the electronics [*Cerni* 1983; *Dye and Baumgardner*, 1984; *Baumgardner*, 1987]. Corrections have not been made for problems in the droplet spectrum due to coincidences, as discussed by *Cooper* [1988] and *Brenguier* [1989], or due to laser beam inhomogeneities [*Baumgardner and Spowart*, 1990; *Wendisch*, 1998]. The principle measurement of the FSSP is drop size, and signals were sorted into 15 equal drop-size bins in the 3-45 μm range. The measurements were summed and recorded every 0.1 s. The dynamic accuracy of the FSSP in measuring LWC and drop size is difficult to quantify. *Baumgardner* [1983] suggests that FSSP measurements of drop size are accurate to 17%, and LWC is accurate to within 34%. However, subsequent evaluations of the FSSP have shown additional potential error terms due to coincidences [e.g., *Cooper*, 1988], inhomogeneities in the laser beam, and effects of airspeed [e.g., *Wendisch et al.* 1996]. In addition, the accuracy of the FSSP appears to depend on factors that are not always quantifiable, such as field calibrations, optical contamination, airflow effects due to position on the aircraft, etc.

The PMS 260X probe sizes particles in 64 channels from 10 μm to 640 μm. According to *Laursen* [1998], 260X data processed by NCAR were filtered to eliminate the first three channels, due to changes in alignment caused by temperature variations. Thus the first usable size channel started at 40 μm. Also, the end element photodiode voltages were monitored for indications that the probe was out of optical alignment, and data were erroneous.

Laursen [1998] also reported that concentrations from the (25 μm) 2D-C and (200 μm) 2D-P image data were suspect and could be in error by a factor of 2. Consequently, only the 2D-C and 2D-P shadow-or counts, were output to the data archives. The shadow-or particle concentrations reported in this paper were obtained by dividing the total counts by the true airspeed. Because there is no image information in the shadow-or measurements, conventional image processing routines that remove "artifacts" (i.e., water streaking on the mirrors and particles that break on the probe tips) cannot be employed, and sample volume corrections for small particles cannot be applied. Additional information describing the C-130 data contained in the FIRE ACE archive can be found in *Laursen* [1998].

The CPI is a relatively new instrument that utilizes innovative technology to record high-definition digital images of cloud particles and to measure particle size, shape, and concentration. The high quality of CPI images supports the generation of individual size distributions for (spherical) water drops and (nonspherical) ice particles. The CPI casts an image of a particle on a solid-state, 1 million pixel CCD camera by freezing the motion of the particle using a 25 ns-pulsed, high-power laser diode. As shown in the conceptual drawing in Figure 1, a particle detection system (PDS) with upstream lasers precisely defines the focal plane so that at least one particle in the image is almost always in focus. Processing of CPI images significantly reduces out-of-focus sizing errors that have plagued the conventional two-dimensional (2-D) imaging probes [*Korolev et al.*, 1998]. Each pixel in the array is 2.3 μm, so particles from about 10 μm to 2mm are imaged. A video-processing engine identifies and sizes particles within the 1 million pixel array, saving only the regions around each image. The CCD camera can run at rates up to 40 Hz, and since more than a hundred particles per frame can be processed, data rates in excess of 1000 imaged particles s^{-1} are obtainable.

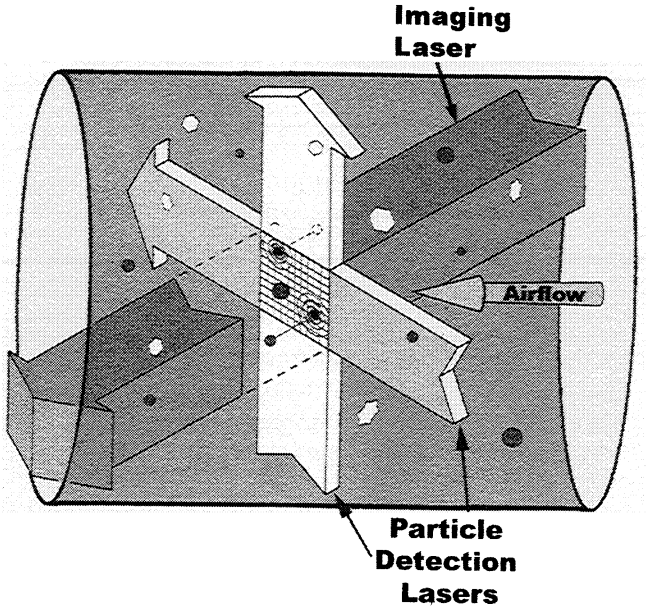

Figure 1. Diagram showing the fundamental design of the Cloud Particle Imager (CPI). See text for explanation of operation.

CPI particle concentration can be computed using a number of methods. Here we describe two nearly independent methodologies and an additional method that uses the 150-500 μm region of the PMS 260X particle size distribution to scale the CPI measurements.

When the CCD camera is being read, the PDS continues to count particles, providing a continuous measurement of total particle concentration (called the "total strobes" measurement of concentration). The total strobes concentration is a function of the threshold level of the PDS, which is user selectable. A check on the effectiveness of the PDS can be obtained by monitoring the number of ("valid") camera frames that actually contain particles. Typically, the PDS threshold is set so that the percentage of valid frames is between 60 and 100%. Since larger particles will more reliably trigger the PDS, there is a roll-off in the particle detection efficiency that starts at about 25 μm and depends on the PDS threshold setting. Thus the small end of particle distributions that are narrow, such as a typical distribution of cloud drops, will be undercounted.

In addition to the in-focus particle that triggers the PDS, high concentrations of small particles in the viewing area may produce additional images that are in various degrees of focus. In this case, the viewing area contains a snapshot of a known volume of particles, and an independent calculation of particle concentration, called the local concentration in this manuscript, can be determined by counting the number of imaged particles, and dividing by the viewing volume. However, the optical depth of field (DOF) and, consequently, the image size and sample volume of the CPI are a function of particle size [see *Lawson and Cormack*, 1995; *Korolev et al.*, 1998]. The CPI particle size distributions shown in this paper have been made using size and sample volume corrections that are done on a particle-by-particle basis. These corrections to the particle size distribution have a major effect on the concentration of small (< ~100 μm) particles. This is possible because CPI images, which contain 256 grey levels, can be used to accurately determine the focus of the image and the distance from the object plane [see *Lawson and Cormack*, 1995].

Because of varying DOF, the imaging sample volume of the CPI varies from about 0.002 to 0.2 cm^3. Local particle concentrations are a true measure within the small volume that is imaged, but they need to be averaged over several tens or hundreds of snapshots to avoid large errors due to sampling statistics. This local concentration is still biased toward the small volumes where the concentration is highest, because the likelihood of triggering is higher where there are more particles. In regions with low particle concentrations, or highly inhomogeneous cloud, the local concentration can be many orders of magnitude greater than the average concentration. Thus the CPI size distributions must be scaled to the average concentration. As a stand-alone instrument, the CPI total strobes average concentration may be used for this scaling. This is most applicable when particle concentrations are relatively low (< ~1000 L^{-1}) and uniform, and the CPI PDS threshold settings are relatively low and unchanging.

When available, the 2D-C (or the 260X as in this study) size distribution is used to scale the CPI size distribution. The 260X measurements were occasionally found to contain noise, even in the mid-sized channels when in clear air, which could be mistaken for actual particle data. The 260X data were therefore compared with time series from the 2D-C shadow-or, CPI and FSSP measurements and inconsistent data were not used. In this study, the 260X size distribution, where it overlaps the CPI size distribution, was used as the first choice for scaling the CPI size distribution (since the PMS 2D-C particle size distributions were not available from the data archives). Where the 260X data were unreliable, the FSSP size distribution was used. This method attempts to make use of the best measurement characteristics of each instrument.

Because of the high resolution of CPI images and the 256 gray levels, it is possible to distinguish spherical from nonspherical particles, depending on the level of focus and size of the particle. Generally, particles that are in good focus and > 50 μm can be distinguished as spherical or nonspherical. This is useful for separating water drops and ice particles in mixed-phase clouds, since ice particles will generally grow to recognizable nonspherical shapes in less than a minute in a mixed-phase cloud. In this study we used a focus algorithm to automatically reject images that were not in sharp focus and then they were classified by another software algorithm that measures the roundness of the image. We also classified several hundreds of particles by eye to verify the accuracy of the automated algorithm. The agreement between the automated and the manual techniques was very good for images >~40 μm. In regions where classification of images < ~40 μm was essential, such as in regions with ice multiplication, a manual classification of particles was implemented. If particles smaller than about 20 μm could not be confidently classified, they were classified as water drops.

4. Arctic Boundary Layer Clouds

4.1. Overview

Sixteen research missions were conducted during FIRE ACE by the C-130. Half of the 16 missions were flown in May 1998 and the remainder were flown in July 1998. Of the

Table 2. Some Characteristics of Clouds Observed on the Sixteen Missions Flown by the NCAR C-130 in May and July 1998

Flight	Date	Temp, °C	Cloud Depth, m	Boundary Layer Cloud?	Mixed From Surface to	Characteristics Observed by CPI
RF01	May 4, 1998	-22 to -25	640 - 1000	yes	1200 m	mixed phase with drizzle and graupel
RF02	May 7, 1998	-18 to -20	290 - 420	yes	400 m	thin mixed phase cloud
RF03	May 11, 1998	-5 to -43	210 - 6600	yes	350 m	ice and mixed layers near boundary layer, very thin patchy water with ice falling from above
RF04	May 15, 1998	-6 to -9	120 - 650	yes	550 m	mostly water with some ice
RF05	May 18, 1998	-7 to -9	180 - 460	yes	150 m	mostly water
RF06	May 20, 1998			no	-	clear
RF07	May 24, 1998	-16 to -21	1500 - 3000	no	-	minimal cloud
RF08	May 27, 1998	0 to -2	<50 - 500 1500 - 1700	yes	250 m	water water
RF09	July 8, 1998	-19 to -28	5650 - 7150	no	-	ice
RF10	July 15, 1998	-2 -20 to -22	<150 4600 - 5200	yes	-	fog - water layers of water and ice
RF11	July 18, 1998	5 to -25	2000 - 6000	no	-	layers of all ice, all water, and mixed
RF12	July 21, 1998	-2	<240	yes	-	no CPI data available
RF13	July 23, 1998	0 to 2 -25	<30 - 280 6150 - 6380	yes	-	water water over ice
RF14	July 26, 1998	2 to -23	Surface - 6500	yes	-	layers of all ice, all water, and mixed
RF15	July 28, 1998	2 to -29	2000 - 6700	no	-	layers of all ice, all water, and mixed
RF16	July 29, 1998	0 to -3	60 - 520 1900 - 2130	yes	-	all water glaciated

16 missions, we identified 11 cases when there were boundary layer clouds. Here we classify a boundary layer cloud as one that is well mixed from the surface to cloud base, or if it has a cloud base that is <300 m. Table 2 shows the flight number, date, temperature, cloud base, cloud top, cloud classification, mixing depth, and some general microphysical characteristics of each of the 16 missions. Upper air soundings were taken from the SHEBA ship approximately every 6 hours. The mixing depth was determined by analysis of the sounding that was closest in time to the flight profile, so some of the fine atmospheric structure may be missed in this analysis. Even so, there appears to be a definitive difference in the subcloud properties in May and July. In May, six out of eight cases had boundary layer clouds, and all six clouds were mixed from the surface to cloud base. The depths of the mixing layers in May ranged from 150 to 1200 m. In July, five of the eight cases had boundary layer clouds, but none of these were mixed from the surface to cloud base.

4.2. Mostly Adiabatic, Homogeneous Water Clouds

The C-130 flew a total of 21 slant profiles on May 15, 18, 27, and July 29 through boundary layer clouds that consisted almost entirely of liquid water. In cloud physics literature, adiabatic generally implies both adiabatic and closed in classical thermodynamics terms; that is, when a parcel of air undergoes an adiabatic ascent from cloud base, it does not exchange mass or heat with its environment. Under these conditions the LWC and temperature can be predicted theoretically from the cloud base temperature and pressure [see *Lawson and Blyth*, 1998]. In addition, the cloud drop size distribution can be estimated using the droplet growth equation [see *Pruppacher and Klett*, 1978]. Basically, during adiabatic ascent the mean drop size will grow monotonically and the drop size distribution will remain monomodal. Bimodal droplet size distributions (not observed in these homogeneous clouds) often result from mixing with environmental air (above cloud top), followed by ascent and activation of new CCN *Jiang et al.* [this issue], present modeling results on the effects of CCN entrainment. In a well-mixed boundary layer the vertical profile of temperature and liquid water content are adiabatic regardless of whether parcels exchange mass with their environment. This is because the parcel and environment are identical.

Figure 2 shows an example of temperature, LWC, and drop size distribution measurements from a boundary layer cloud observed on May 18, 1998, which is mostly adiabatic and homogeneous. In the example shown in Figure 2, the temperature profile is nearly adiabatic, the profile of LWC measurements from the King probes and PVM are within 20% of adiabatic. (The FSSP LWC is about twice the adiabatic value and is believed to be in error, as discussed in section 4.3.) The FSSP drop size distribution is monomodal, the profile of mean droplet size increases monotonically with height, and the dispersion of the droplet spectrum is constant with height. There was no drizzle detected. All of these factors support the conclusion that this boundary layer cloud observed from 2208-2210 UTC by the C-130 on May 18, 1998, was mostly adiabatic.

CPI images provide another method of investigating cloud homogeneity. As seen in Figure 1, when a particle is detected by the PDS and the CPI imaging laser is fired, the imaged volume may contain more than one particle, particularly if the particle concentration is relatively high. In a homogeneous cloud, the effect of sampling random volumes of equal size

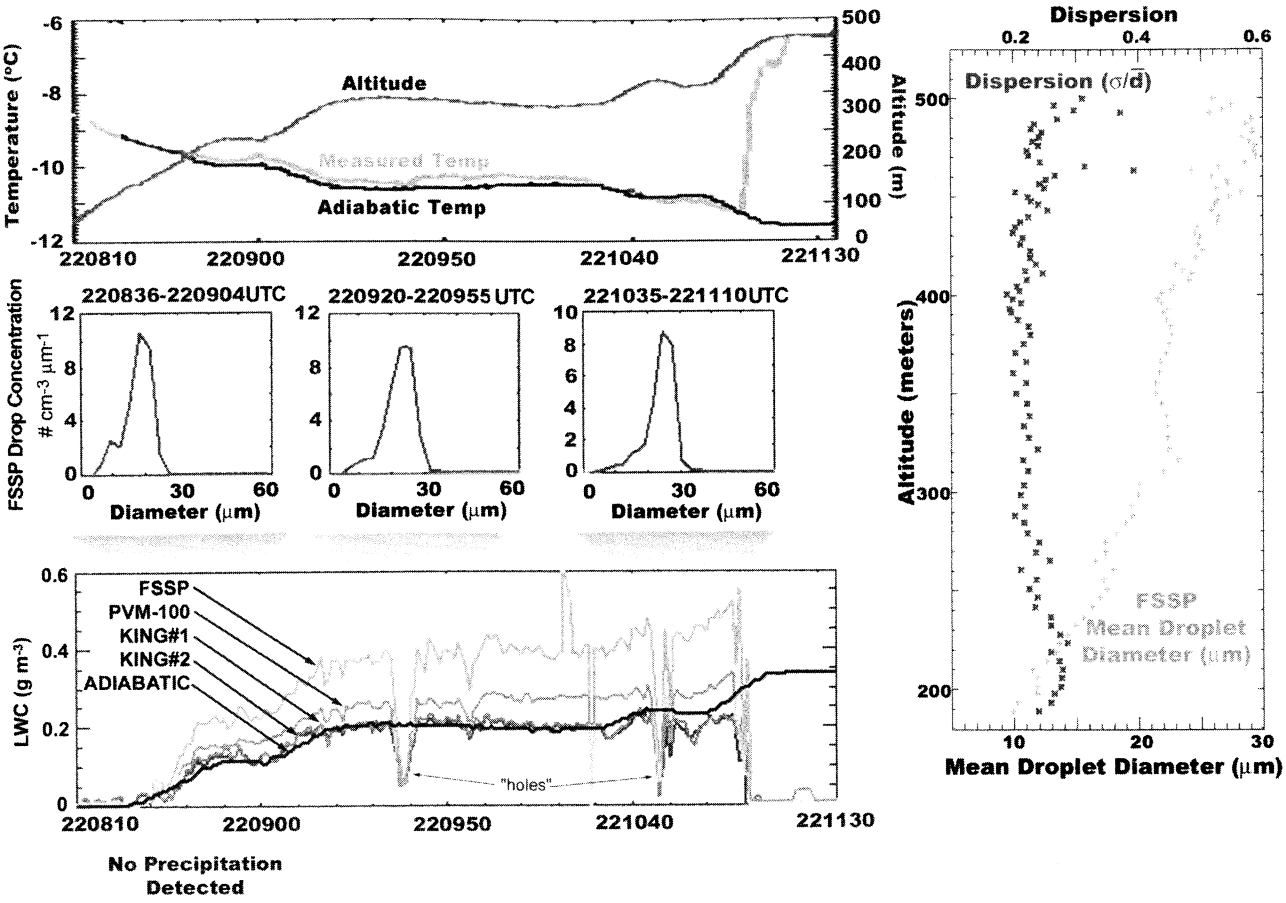

Figure 2. (top) Temperature and altitude recorded by the C-130 on May 18, 1998, as it sampled a boundary layer cloud and the calculated adiabatic temperature. (middle) Forward Scattering Spectrometer Probe (FSSP) size distributions for different time periods. (bottom) A time series of liquid water content (LWC) recorded by several different probes is compared to the calculated adiabatic value. (right) The FSSP mean droplet diameter and dispersion are plotted versus altitude.

would result in a Poisson distribution for the number of particles per sample. Figure 3 (top) shows the Poisson distribution for the number of particles per sample with the same mean as that observed by the CPI from 2210:10 - 2210:30 UTC during the slant profile shown in Figure 2. Also shown in Figure 3 (top) is the distribution of the number of particles per image frame actually measured by the CPI. The comparison in Figure 3 (top) shows that the CPI measurements closely follow the theoretical Poisson distribution.

A more sensitive test for inhomogeneity can be made by conditional examination of the particle size distributions for the cloud region shown in Figures 3 (top). One conditional distribution was made of the sizes of particles imaged in CPI image frames with three or fewer particles, while the other was made from the sizes of particles imaged in frames with five or more particles. If the cloud were homogeneous, the conditional size distributions should be identical. The data in Figure 3 (bottom) show that the conditional spectra are nearly identical, suggesting that this region of cloud was quite homogeneous.

The measurements shown in Figures 2 and 3 are representative of FIRE ACE boundary layer clouds with adiabatic LWC profiles. However, even in these cases, there is evidence that some entrainment and mixing is occurring in some regions of the cloud. In Figure 2, clear air holes are seen which extend to at least 100 m below cloud top. The CPI also confirms the lack of cloud in these spots. Presumably, these are entrainment events that bring clear air from above the cloud into the cloud layer. *Curry* [1986] also observed that cloud top air penetrated downward into the cloud to a depth of at least 50 m.

4.3. Evaluation of LWC Instrumentation in Adiabatic Clouds

In addition to providing an excellent natural outdoor laboratory for studying mixing and evolution of the droplet spectra, these Arctic clouds provide a reliable test bed for assessing the performance of some of the microphysical instrumentation. The LWC profile and temperature are predictable in regions of cloud that have ascended adiabatically from cloud base to the observation level [e.g., *Jensen et al.*, 1985; *Lawson and Blyth*, 1998]. The cloud base temperature and pressure were measured at the point where the FSSP droplet concentration exceeded zero on ascents and when the concentration dropped to zero on descents. A zero FSSP concentration threshold was used because, unlike some environments where there are relatively high concentrations of large aerosols that produce occasional counts, the FSSP

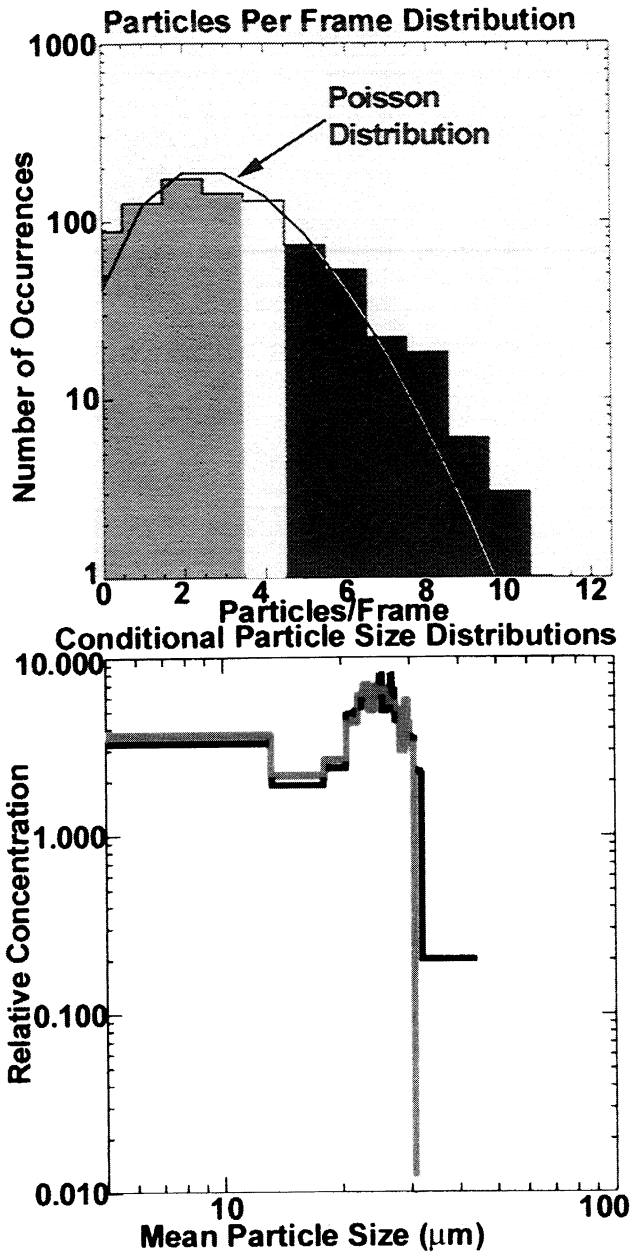

Figure 3. (top) Histograms of the number of particles per frame for all the CPI imaged frames during the time period 2209:45 – 2210:25 shown in Figure 2 along with the Poisson distribution with the same mean, and (bottom) conditional particle size distributions produced by using only those particles in frames with five or more particles (black) and by using those particles in frames with three or fewer particles per frame (grey).

almost always read zero in clear air. This method of computing adiabatic LWC is not only the simplest to implement but, arguably, also the most accurate, because the subsequent analysis depends primarily on relative changes in temperature and pressure. Static pressure measurements on research aircraft are generally felt to be accurate to < 1 mbar. In dry air an absolute uncertainty of about 0.3°C is expected in the Rosemount temperature measurements [*Lawson and Cooper*, 1990]. *Lawson and Cooper* show that an additional error from sensor wetting of < ~0.5°C is expected when the LWC is < ~0.5 g m^{-3}, as was the case in these clouds. No evidence of temperature spikes, typically found when the Rosemount temperature probe element gets wet [*Lawson and Cooper*, 1990], was observed on cloud exit. For a 1°C error in measurement of temperature and a 1 mbar error in pressure at cloud base, there is only a 0.025 g m^{-3} maximum error in adiabatic LWC for conditions typical of FIRE ACE boundary layer clouds. Thus instrumentation measurement errors in pressure and temperature at cloud base can be expected to have an insignificant contribution to the determination of adiabatic LWC.

Figure 4 shows scatterplots of LWC measurements versus adiabatic LWC for all of the (nine) ascents and descents through clouds that were determined to be close to adiabatic, although as shown in Figure 2, "holes" were occasionally observed in these clouds. Since there is no reason to expect superadiabatic LWC in these clouds and since there is evidence of some mixing almost everywhere, the calculated adiabatic value is the maximum that the measurements should reach (except for the contribution from measurement errors). The data in the scatterplots show that both King probes generally did not exceed the adiabatic value and were within 75% of adiabatic LWC (except in regions with obvious "holes"). The PVM scattered around the adiabatic value and sometimes exceeded it by up to about 35%. The FSSP generally exceeded the adiabatic LWC value by up to a factor of 2.

While instrumentation errors were shown to have a negligibly small effect in determination of adiabatic LWC, fluctuations in the actual cloud base level could potentially introduce significant errors in adiabatic LWC. For example, during a slant ascent or descent through a stratus cloud, the aircraft may enter cloud base at one point, and when it reaches cloud top, the air parcel it samples may have originated at a different cloud base elevation. Significant errors in adiabatic LWC are more likely when there are noticeable undulations in

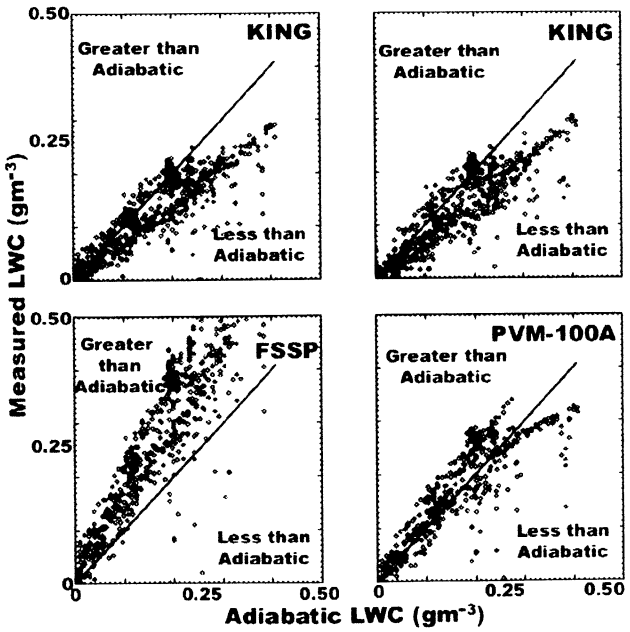

Figure 4. A scatterplot of measured liquid water contents (for four instruments) taken during nine different slant profiles plotted against the calculated adiabatic values.

cloud base elevation. Figure 5 shows LWC measurements from one of the nine adiabatic profiles and the effect on LWC for different cloud base elevations. It can be seen that a deviation from the measured value of 1001 mbar to about 1013 mbar (a difference of about 120 m) would be required to produce an adiabatic LWC that agrees with the peaks in the FSSP measurements. It is very unlikely that variations of this magnitude existed in the actual cloud base elevations in this case, as evidenced by the measurements of FSSP and PVM LWC also shown in Figure 5, when the C-130 exited cloud and flew level just underneath cloud base for about 15 s. If a lower cloud base existed, it would probably have been detected during this horizontal leg. In addition, after exiting cloud, the C-130 flew for about 2 min just below the cloud base elevation before climbing for another cloud penetration. During this time, there was no indication of lower cloud base, and the cloud base measured upon ascent was within 2 mbar of the previous measurement. The nine slant profiles used to generate the data in Figure 4 were carefully selected, so that errors in determination of cloud base were minimized.

Thus we can conclude that for C-130 measurements from this field project (1) the King probes rarely exceeded the adiabatic value and were usually accurate to within 20%, (Shortly after this manuscript was accepted, measurements of the dimensions of the King probe sensor wires used in the

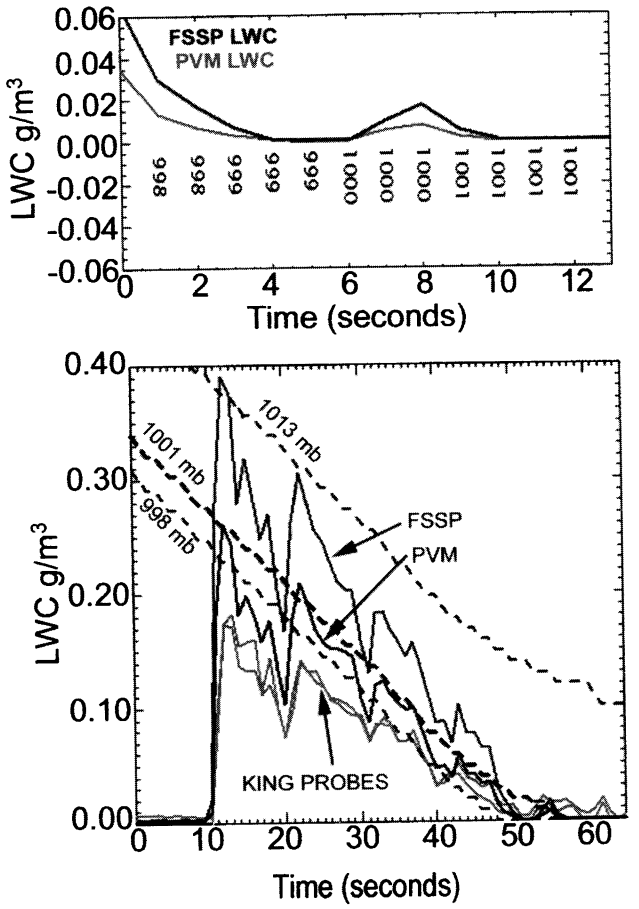

Figure 5. (top) Liquid water content versus time and pressure as the C-130 entered the adiabatic cloud from below. (bottom) Measured liquid water content versus time compared with the calculated adiabatic LWC profile assuming different cloud bases.

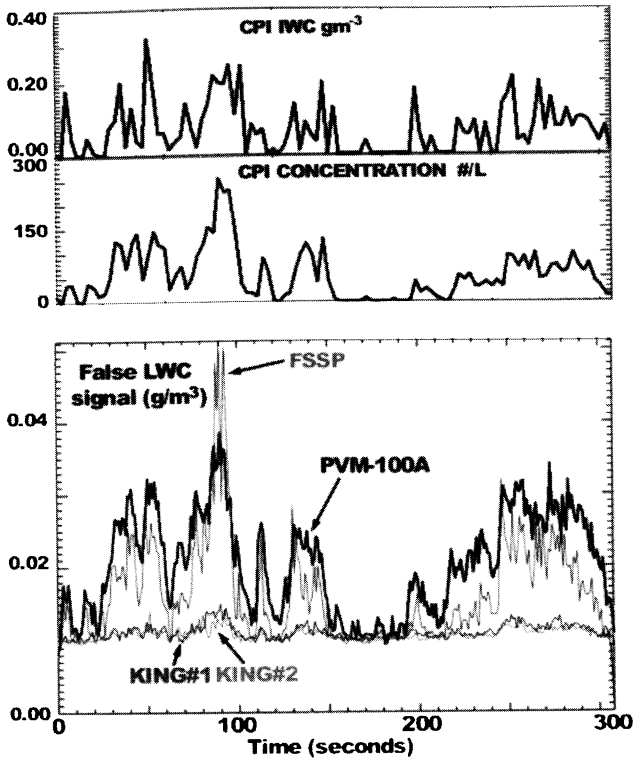

Figure 6. CPI IWC and concentration are shown along with the false LWC signal observed by the FSSP, particulate volume monitor (PVM), and King probes.

FIRE ACE project showed that the area of the sensor was overstated by about 20%. In the calculation of LWC, sensor area is inversely proportional to LWC, so the FIRE ACE measurements would increase by about 20%. The NCAR Research Aviation Facility (RAF) plans to publish a correction that can be applied to the archived FIRE ACE data (K. Laursen, personal communication, 2000). The end result will be that the King LWC measurements will be increased by about 20% and be in closer agreement with the PVM values.) (2) the PVM measurements scattered around the adiabatic value, with an occasional apparent tendency to overestimate the adiabatic LWC, and (3) the FSSP measurements are heavily biased toward values that exceeded the adiabatic LWC. It is highly unlikely that the FSSP measurements could be the result of underestimates in the adiabatic LWC, since this would mean that the aircraft consistently measured a cloud base that was about 10 mbar too high and that the King and PVM probes consistently underestimated LWC.

The FSSP counts and sizes droplets. Errors in sizing are raised to the third power and can result in significant errors in LWC. The NCAR FSSP was calibrated with glass beads in the field, but even so, sizing errors can occur [*Baumgardner et al.*, 1990]. Errors from undercounting in high (> 600 cm^{-3}) drop concentrations are due to coincidence, which also artificially broaden the drop size spectra [*Cooper*, 1988; *Brenguier*, 1989]. Coincidence artificially increases LWC because two small drops are erroneously recorded as one larger drop, and since LWC is proportional to the third moment, the undercounting is outweighed by the increase in drop size. However, drop concentrations rarely exceeded 250 cm^{-3}, except perhaps downwind of the effluent plume from

the SHEBA ship (for information on aerosols during SHEBA, see *Yum and Hudson*, [this issue] and *Pinto et al.*, [this issue]), so coincidence errors should not be problematical. Thus there is currently no explanation for the apparent overestimation of LWC observed in the FSSP measurements.

Regardless of the apparent error in FSSP measurement of LWC, the primary function of the FSSP is to measure drop size distribution. There is currently no determination of how much of the apparent error in FSSP LWC is due to error(s) in sizing and/or concentration. However, FSSP measurements that show comparisons of relative FSSP drop size distributions are still very useful and are included frequently in this paper.

The FSSP displayed the most stable baseline outside of cloud and was the best probe to use to identify cloud boundaries. The baseline of the King probes often varied erratically by up to $\pm$ 0.05 g m^{-3}. The PVM baseline also drifted occasionally, although the drift was slower and did not fluctuate rapidly. Care must be taken to subtract the clear-air offset from both the King and the PVM probes. All four probes were inoperative during some flights and/or portions of flights; however, there were two King probes and one or the other probe was operational on every flight.

A qualitative investigation of the effects of ice on measurements of LWC was undertaken by comparing probe responses in a cirrus cloud with all ice particles. Figure 6 shows the responses of the King, PVM, and FSSP probes to an all-ice cirrus cloud, along with ice particle concentration and IWC measurements derived from CPI measurements. There are undefined uncertainties in the CPI IWC measurements, however, using the relative responses of the LWC instruments, it can be seen that the FSSP and PVM (optical) probes respond much more to ice than the King (hot wire) probes. The CPI IWC was dominated in this cirrus cloud by the larger (200 to 400 μm) bullet rosette crystals (shown later in Plate 5). Conversely, the small (< 50 μm) ice particles made up the majority of the CPI concentration measurements. The relative phasing of the PVM and FSSP LWC measurements agree better with the CPI concentration (small particles) than the CPI IWC (larger particles), suggesting that the false LWC signals of the FSSP and PVM probes in an all-ice cloud are affected more by the small particles.

4.4. Nonadiabatic, Inhomogeneous Clouds

As previously discussed, nine of the 21 slant profiles flown through the nearly all-water boundary layer clouds were found to be mostly adiabatic and homogeneous. Here we discuss microphysical properties of typical examples from the remaining set of 12 clouds, which were nonadiabatic, inhomogeneous, and actively mixing.

Figure 7 shows a C-130 slant profile through a boundary layer cloud on July 29, 1998. Both LWC and temperature display a systematic trend to deviate increasing more from adiabatic values with increasing distance above cloud base, which strongly suggests an active mixing process at cloud top. At cloud top, the temperature fluctuates strongly and is often warmer than adiabatic, due to entrainment of relatively warm air from the temperature inversion above cloud top. The droplet spectra are bimodal at cloud top, and drizzle was encountered lower in the cloud. This is in contrast to boundary layer clouds where the LWC and temperature profiles were adiabatic and the drop spectra were monomodal (i.e., Figure 2), where drizzle was not observed anywhere along the profile.

When the LWC and temperature profiles were significantly subadiabatic in FIRE ACE boundary layer clouds, the droplet spectra near cloud top were often bimodal, and drizzle was observed lower in the cloud. It was not a necessary condition for the drop spectra to be bimodal to observe drizzle, since in some subadiabatic clouds that were actively mixing, drizzle was occasionally observed at cloud base without concurrent measurements of bimodal drop spectra in the cloud. However, it should be remembered that the aircraft samples a relatively small volume of cloud, and bimodal drop spectra could be present at locations in the cloud not sampled by the aircraft.

Figure 8 shows another profile flown about 7 minutes earlier than the slant profile in the same boundary layer cloud shown in Figure 7. Basically, the same large-scale observation seen in Figure 7, which is that the boundary layer cloud is actively mixing at cloud top, is seen in Figure 8. The profile shown in Figure 8, however, has regions where the C-130 flew several-minutes-long constant altitude legs, providing an opportunity to examine cloud inhomogeneity using the conditional spectra technique introduced in section 4.2 and shown for a relatively homogeneous cloud region in Figure 3. The presentations of theoretical Poisson and CPI measured number of particles per image frame and the conditional drop size distributions, analogous to those shown in Figure 3, are shown above the time series measurements in Figure 8. The measured number of particles per image frame follow the Poisson distribution, and the conditional drop size distributions are nearly identical for the cloud regions at 180 and 270 m mean sea level (msl). This implies that these regions are well mixed, and there is not a large degree of inhomogeneity in the lower and middle levels of this boundary layer cloud. On the other hand, near cloud top at 450 m msl, a larger degree on inhomogeneity can be seen in the temperature and LWC measurements, and this is reflected in the conditional drop size distribution measurements, which are noticeably different. It is interesting to note that the trend in the conditional spectra is for the smaller droplets to be found in locally higher concentrations than the larger droplets. Just the opposite might be expected in an actively mixing cloud.

It is also interesting to note that the drop size distribution is distinctly bimodal in the midlevel region, yet the conditional spectra revealed no inhomogeneity. This suggests a process whereby the mixtures formed at cloud top (cooled by evaporation), descended toward midcloud, and continued mixing while descending, which resulted in a relatively well mixed region.

Perhaps the most striking aspect of boundary layer clouds observed during FIRE ACE, as revealed by this analysis, is how a group of clouds which are fairly similar in visual appearance, can exhibit such variability in microphysical properties. To investigate further aspects of the FIRE ACE boundary layer clouds, we generated time series measurements of key microphysical, thermodynamic, and dynamic parameters for six cases.

Figures 9 and 10 show time series measurements of LWC, temperature, vertical velocity, FSSP concentration, altitude, and the standard deviation for all of these quantities except for altitude. The data in these figures are organized to show

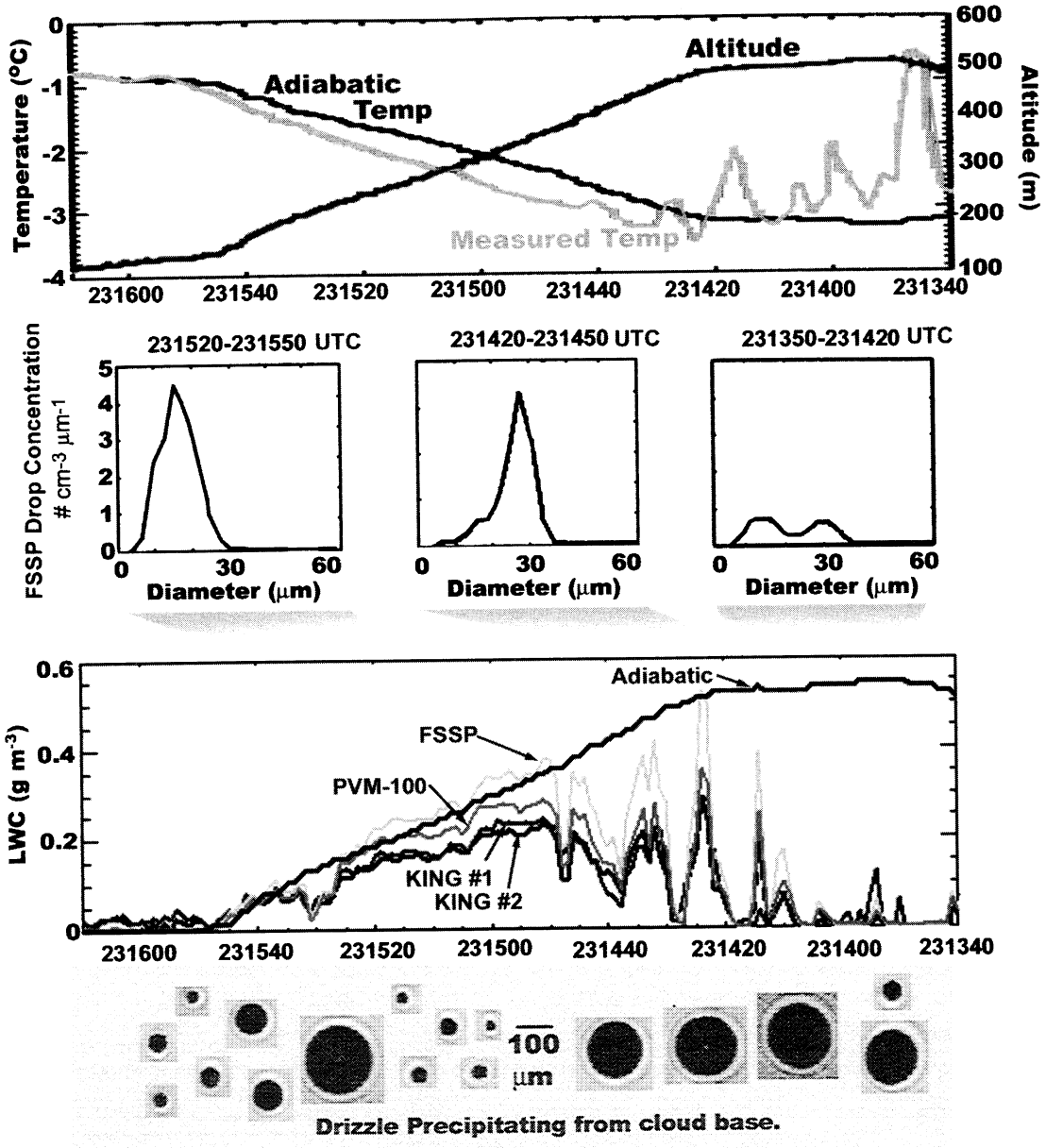

Figure 7. (top) Time series of the temperature and altitude recorded by the C-130 on July 29, 1998, as it sampled a boundary layer cloud and the calculated adiabatic temperature. (middle) FSSP size distributions for different time periods. (bottom) A time series of LWC recorded by several different probes is compared to the calculated adiabatic value.

examples of the microphysical variability between these boundary layer clouds. The regions selected for display in Figures 9 and 10 were chosen when the C-130 flew level for several seconds and at different altitudes in the boundary layer clouds (the only exception being May 15 in Figure 9 when there were no representative level regions). The purpose of selecting these regions was to see if there were any consistently recognizable features that varied as a function of altitude in the boundary layer clouds. Figure 9 shows examples of cloud regions (also shown in Figures 2 and 4) which were mostly adiabatic with relatively constant FSSP drop concentration and temperature measurements. These clouds displayed monomodal droplet spectra, and there were no observations of drizzle at the time of the in situ measurements. Figure 10, on the other hand, shows cloud regions where mixing produced subadiabatic LWC, variations in the FSSP drop concentration and temperature, and often bimodal droplet spectra and drizzle.

The data in Figure 9 show that there is very little change with altitude in the thermodynamic (i.e., temperature), dynamical (i.e., vertical velocity), and microphysical parameters (i.e., LWC and FSSP concentration) in these all-water clouds. As shown in Figure 3, the droplet spectra were monomodal and no drizzle was observed by the C-130. As previously stated, this is typical of the "mostly adiabatic" boundary layer clouds. The values of standard deviation (σ) in Figure 9 are mostly constant, except for the bumps in drop concentration and LWC (resulting from the 20 s over which σ is computed) around the region where the "holes" are observed in the May 18 cloud.

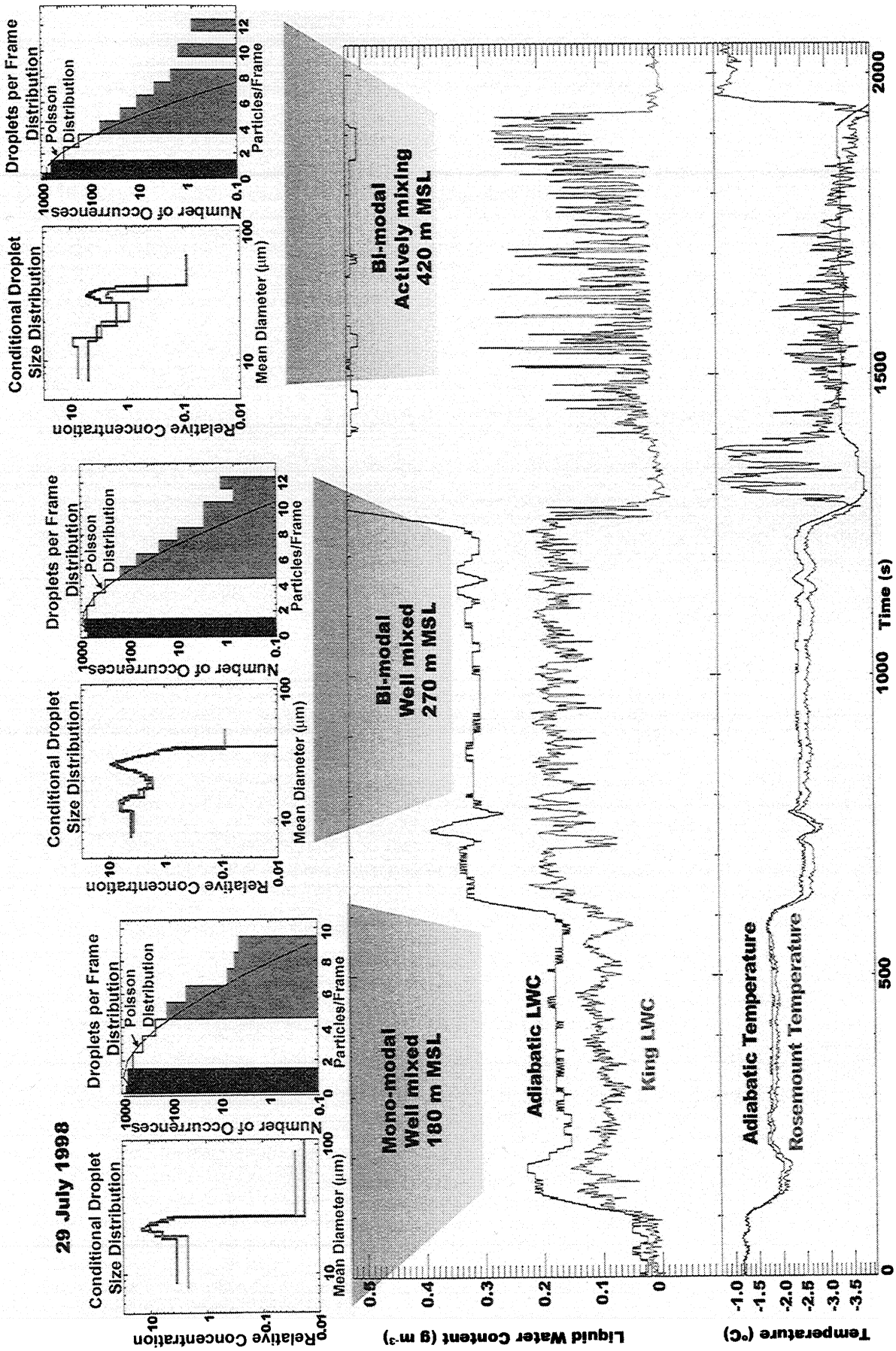

Figure 8. Time series of measurements from a boundary layer cloud on July 29, 1998. Conditional size spectra (as shown in Figure 3) for each region are shown above.

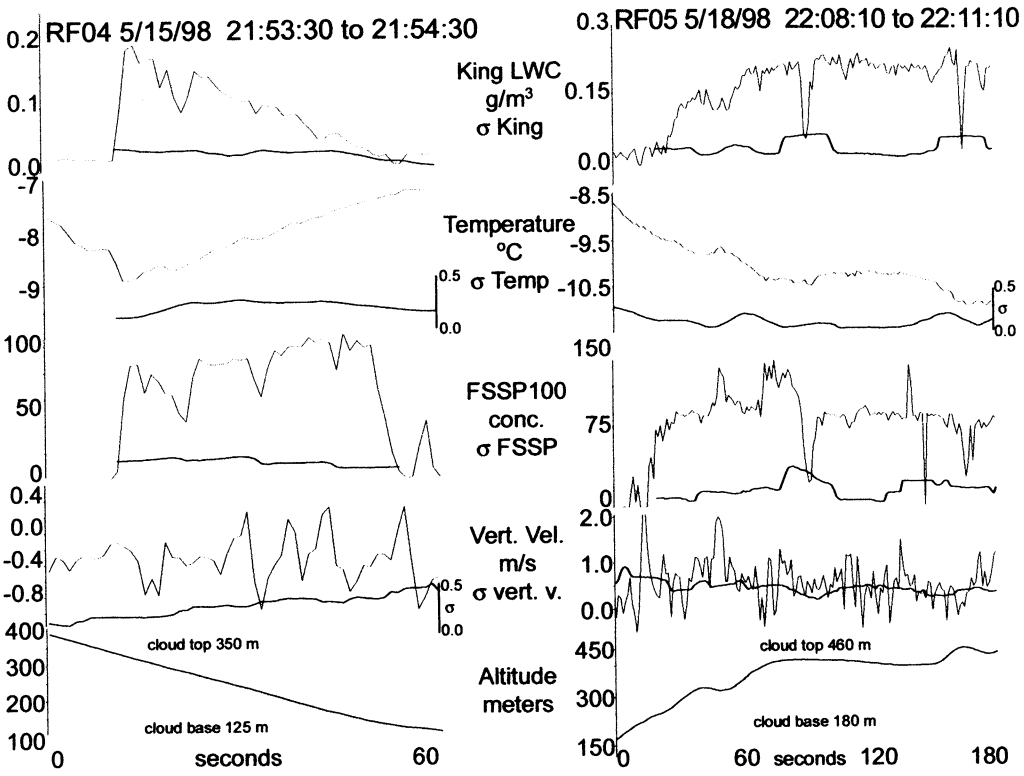

Figure 9. Time series of measurements and their standard deviations made by the C-130 as it passed through two boundary layer adiabatic clouds.

Figure 10 shows four examples of profiles in boundary layer clouds that were actively mixing. The data in this figure show that fluctuations in temperature, LWC, and FSSP drop concentration tend to increase as the C-130 gets closer to cloud top. This is consistent with the hypothesis put forth previously that these boundary layer clouds are mixing from the cloud top downward. The measurements in Figure 10 show that there is not an increase in the standard deviation of vertical velocity with height in these boundary layer clouds. The air motion system in the C-130 contains a residual offset that is on the order of 0.5 m s^{-1}, so the small offset in vertical velocity in Figures 9 and 10 should be ignored. However, the small-scale fluctuations are considered to be accurate to within a few tenths m s^{-1}, so the consistent lack of increase in the fluctuation of vertical velocity with height is significant. The boundary layer clouds depicted by the measurements in Figure 10 all had bimodal drop distributions at cloud top, and drizzle was observed below cloud.

Generally, in Figures 9 and 10 there was a lack of correlation in vertical velocity with FSSP drop concentration, and there is a correlation between LWC and drop concentration. An exception to the above generalizations is seen in Figure 9 on May 18, where the drop concentration increases from the nominal level of about 80 cm^{-3} to 140 cm^{-3} in three regions, and the LWC remains fairly steady. In these regions the vertical velocity shows a significant increase. The FSSP mean drop size (not shown) was anticorrelated with drop concentration, which accounts for the lack of increase in LWC, and also agrees with the observation that a localized updraft could have activated more CCN.

The test for inhomogeneity using CPI images, described in section 4.2 and shown in Figures 3 and 8, was applied to the region in Figure 9 on May 18 where there is a subtle but noticeable variation in drop concentration. Figure 11 shows the results in the same format as Figure 3. which is from the same cloud profile as shown in Figure 11 but about 50 s later when there was no obvious variation in droplet concentration. The conditional spectra in Figure 11 are slightly separate, suggesting that the region has a detectable inhomogeneity. The results of the inhomogeneity test using CPI image data shown in Figures 3 and 11 demonstrate the sensitivity of this type of test but do not provide information on the scale of the inhomogeneity. However, in this case, the large-scale structure that can be seen in the time series measurements of Figure 9, probably caused the separation seen in Figure 11. The tendency for smaller droplets to be observed in higher concentration regions is consistent with the time-series measurements.

4.5. Mixed-Phase Cloud

Figure 12 shows an example of time series measurements from a boundary layer cloud that is fairly unique in the C-130 FIRE ACE data set. This was a case where cloud base was higher (640 m msl) than the clouds previously discussed, and the entire subcloud layer was well mixed to the surface (see Figure 12). This was the first C-130 mission (May 4), the atmosphere was still transitioning from the winter regime, and with the higher cloud base, this boundary layer cloud was colder than the other cases discussed. The trends in the measurements in Figure 12 differ from Figures 9 and 10 in that the standard deviation in vertical velocity is noticeably larger lower in the cloud, and LWC is less near cloud top than near cloud base. Even though the LWC measurements are significantly less than adiabatic everywhere in this cloud,

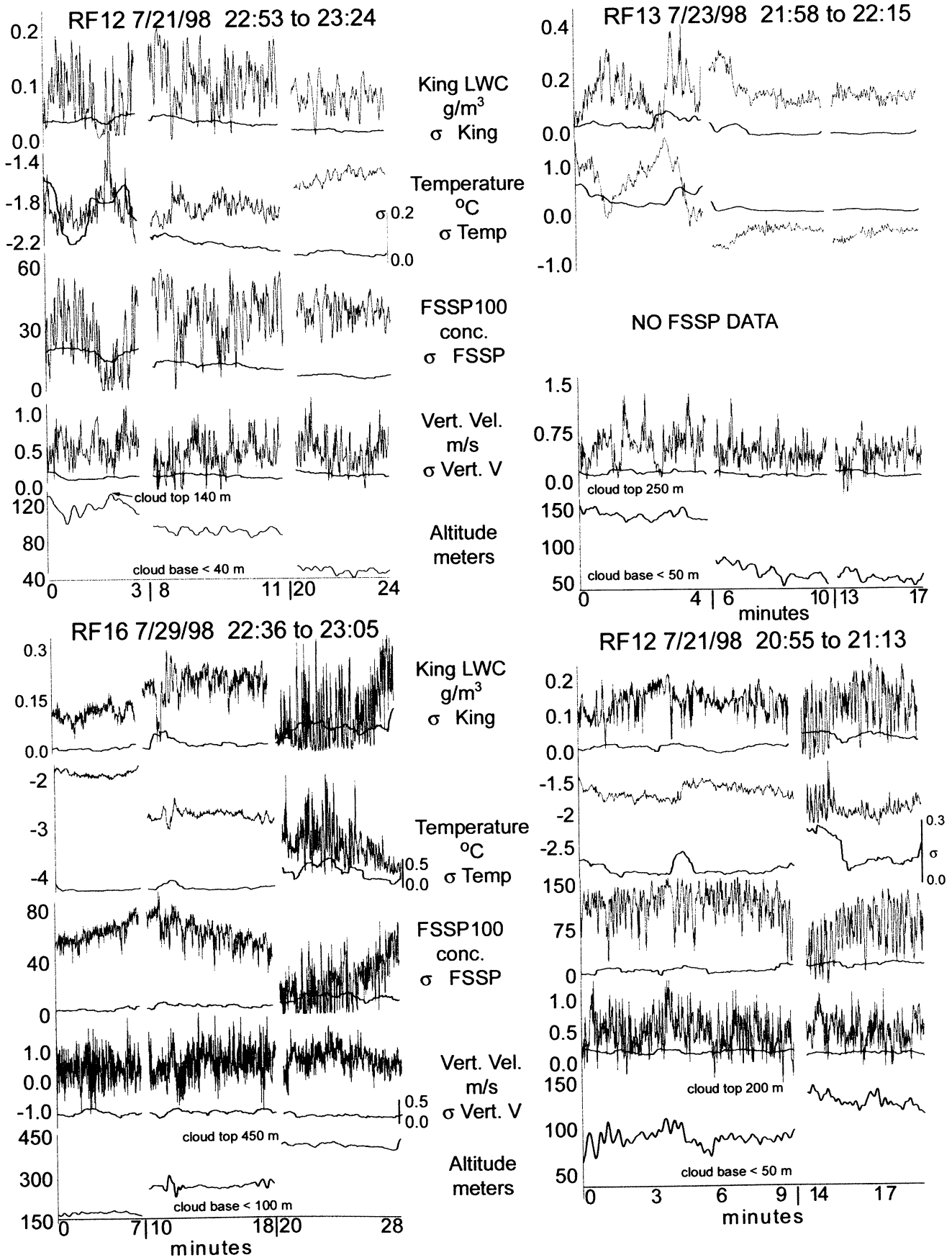

Figure 10. Time series of measurements and their standard deviations made by the C-130 as it flew different level passes through boundary layer clouds on four different occasions.

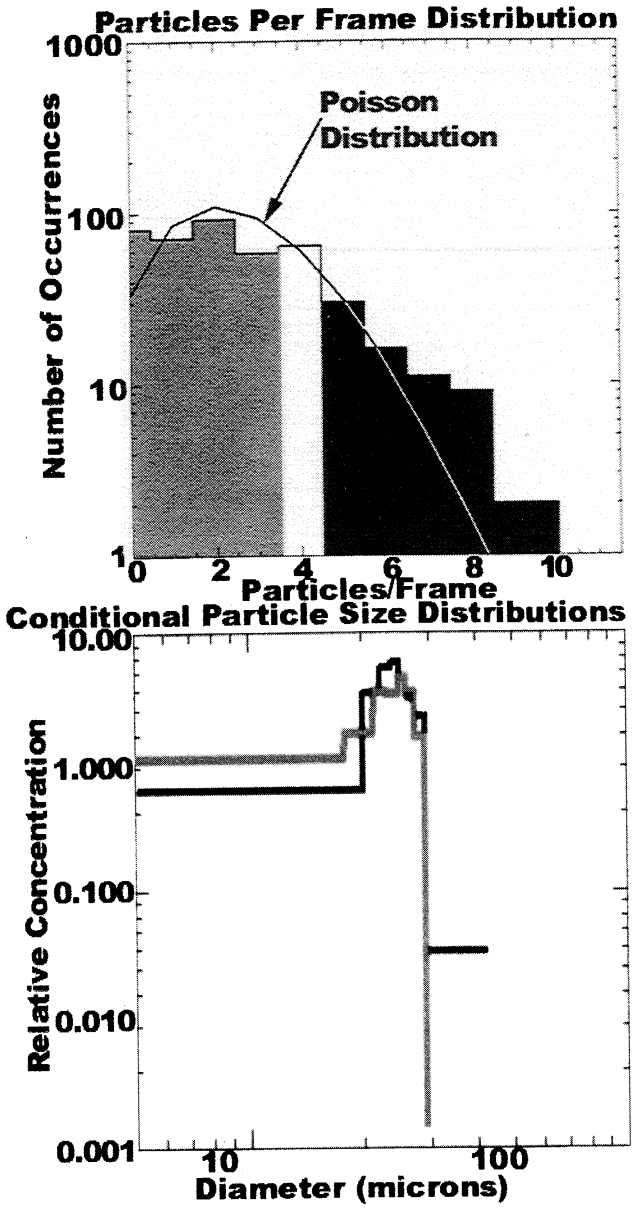

Figure 11. (top) Histograms of the number of particles per frame for all the CPI imaged frames during the time period 2209:00 – 2209:40 shown in Figures 2 and 9 along with the Poisson distribution with the same mean, and (bottom) conditional particle size distributions produced by using only those particles in frames with five or more particles (black) and by using those particles in frames with three or fewer particles per frame (grey).

there is no evidence that active mixing near cloud top and the drop spectrum (not shown) at cloud top is monomodal.

The most striking feature of the boundary layer cloud observed on May 4 is the inhomogeneity in the hydrometeor fields. Plate 1 shows a portion of the flight track when the C-130 was descending and making passes over the SHEBA ship, from cloud top (1025 m) down to cloud base (690 m), and examples of CPI images, water drops, and ice particle size distributions during this time period. The data in the figure show that the hydrometeor fields varied considerably over spatial distances of 10 km horizontally and a few hundred meters vertically. When the C-130 skimmed cloud top and then turned and made a pass 30 m below top, it encountered a mixture of small (<30 μm) ice particles and supercooled (-25.5° to -22°C) cloud droplets. The King LWC registered about 0.15 g m^{-3}. The CPI recorded images of only a few 100 - 250 μm ice particles, which may have fallen from a higher cloud. Some of the CPI images of small ice particles are difficult to distinguish from (spherical) cloud drops. However, a large percentage of the images of small particles that were classified as ice were obviously nonspherical. Laboratory experiments have shown that particles have a linear growth rate of a few tenths of a micron per second at -25°C in a water saturated environment [*Pruppacher and Klett* 1978]. Frozen drops would therefore be expected to grow to recognizable (~100 μm) ice particles within a few minutes. Thus, the relatively high (~1000 L^{-1}) concentration of ice particles near cloud top probably reflects a region where ice nucleation recently occurred.

On the next pass 75 m below cloud top, Plate 1 shows that the CPI water drop spectrum had broadened slightly. The total concentration decreased from about 1000 L^{-1} to 60 L^{-1} and more large ice particles were observed, mostly unrimed with sizes to about 300 μm, with an occasional rimed particle as large as 600 μm. However, just west of this position and 30 m lower (920 mbar), while the C-130 was turning to reverse course, a section of drizzle about 10 km in horizontal dimension was observed with supercooled (-25°C) drops with sizes up to 180 μm. After the pocket of drizzle was transected, the C-130 made another pass over the ship while descending to 900 m and encountered supercooled drops with a mode of about 30 μm and ice particles that were mostly < 500 μm, with a few larger rimed particles. However, when the C-130 reversed course and 2 minutes later flew only 30 m lower (870 m) over the same flight track, significantly higher concentrations of rimed ice particles from 400 to 800 μm and occasional graupel particles up to 1 mm were observed.

The degree of inhomogeneity in cloud microphysics could possibly be due to mixing downward from cloud top or from the effects of seeding from higher clouds. Even though significant concentrations of ice particles were not observed during the passes over cloud top, the potential for temporal and spatial variability of this type of seeding precludes eliminating this possibility. The presence of the small pocket of drizzle at -25°C, however, cannot be directly explained by either surface or elevated effects. *Curry* [1986] reported drizzle when there was a relatively large dispersion in the drop spectra. In this case the FSSP drop spectra at cloud top were relatively narrow and monomodal, in contrast to the example shown in Figure 7, where the drop spectra were bimodal and drizzle was observed at -1°C. However, the C-130 could not completely investigate cloud top, so bimodal drop spectra may have existed somewhere at cloud top. The cloud on May 4 existed for a long time, and seeding from above was sporadic. The curious pocket of drizzle, which was produced by coalescence, may have been an older region that was not seeded from above.

5. Deep Stratus Cloud With Very High Ice Particle Concentrations

Next, we examine inhomogeneity in microphysical measurements collected in a deep Arctic stratus cloud. This is not a boundary layer cloud according to the definition used in this

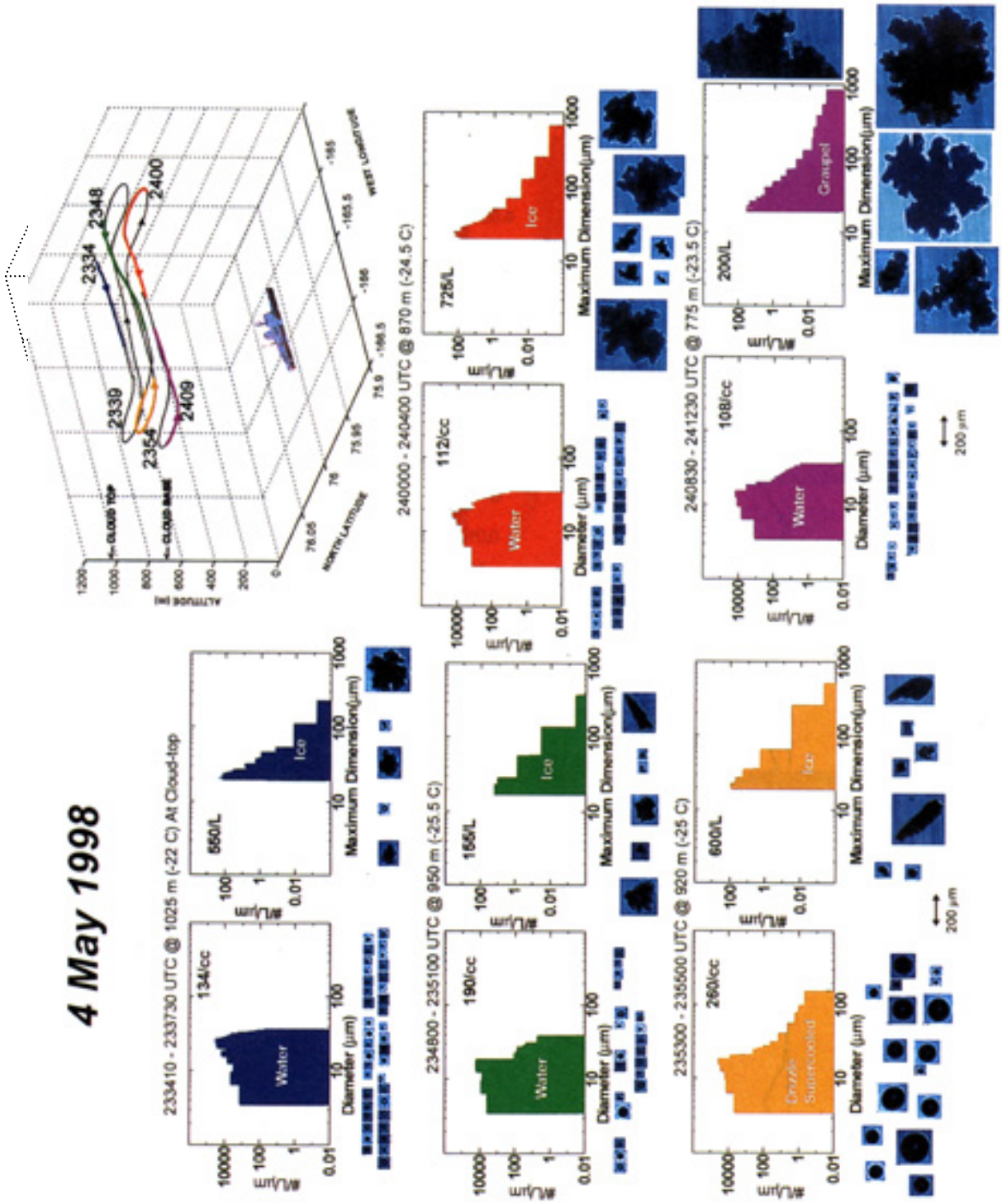

Plate 1. Example of a boundary layer cloud with extremely variable hydrometeor fields that exist over relatively small (10 km) spatial distances. The 3-D flight track is for the NCAR C-130 as it descended over the SHEBA ship. The times shown on the track correspond to the CPI-derived particle size distributions of ice and the combined CPI-FSSP water drop size distributions in the mixed-phase clouds. Sample CPI images are shown for each particle size distribution.

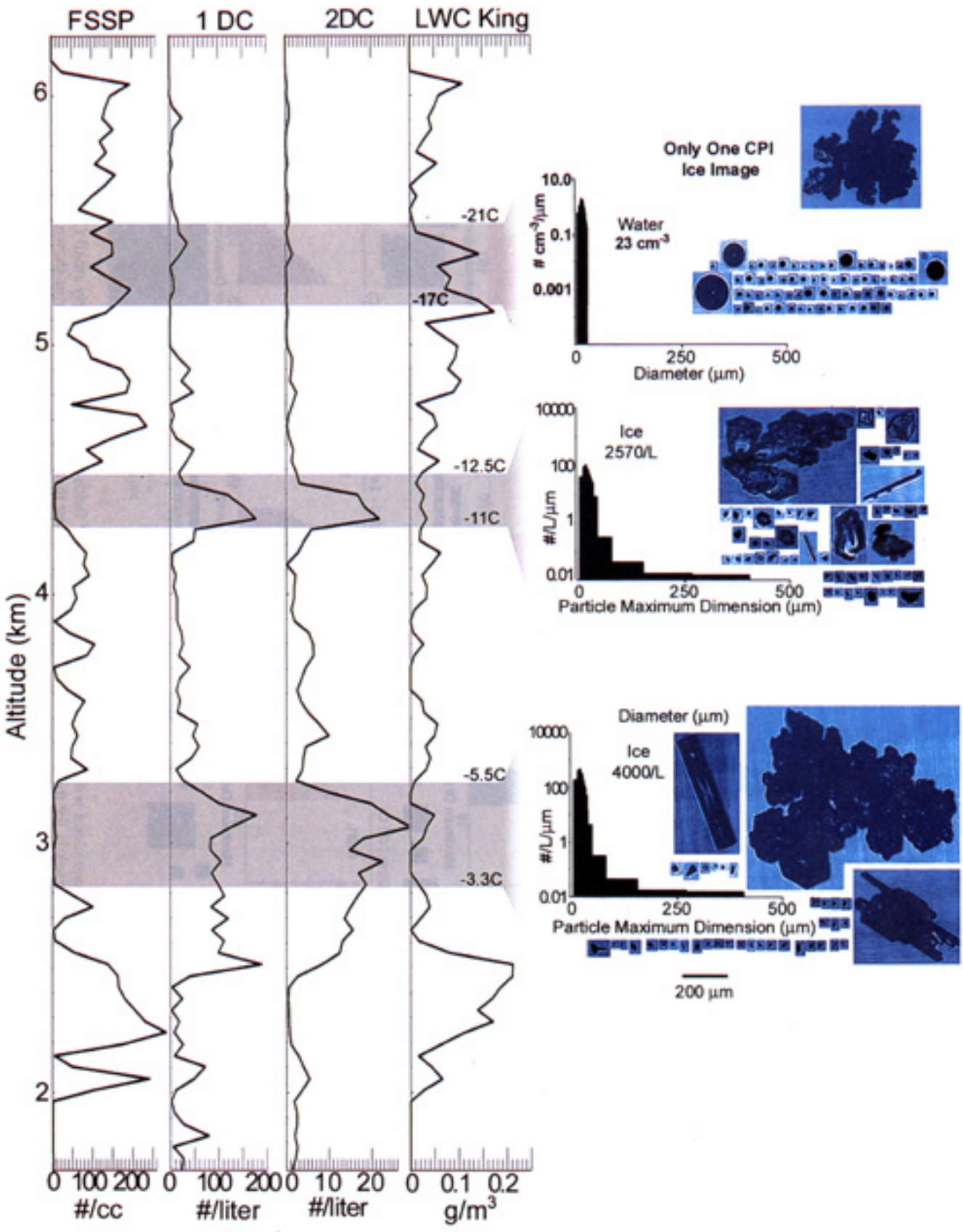

Plate 2. Concentrations measured by the FSSP, 1D-C, and 2D-C, are plotted with the King LWC versus altitude for a thick stratus cloud observed on July 18, 1998. CPI particle size distributions for ice and water as well as example images are shown to the right.

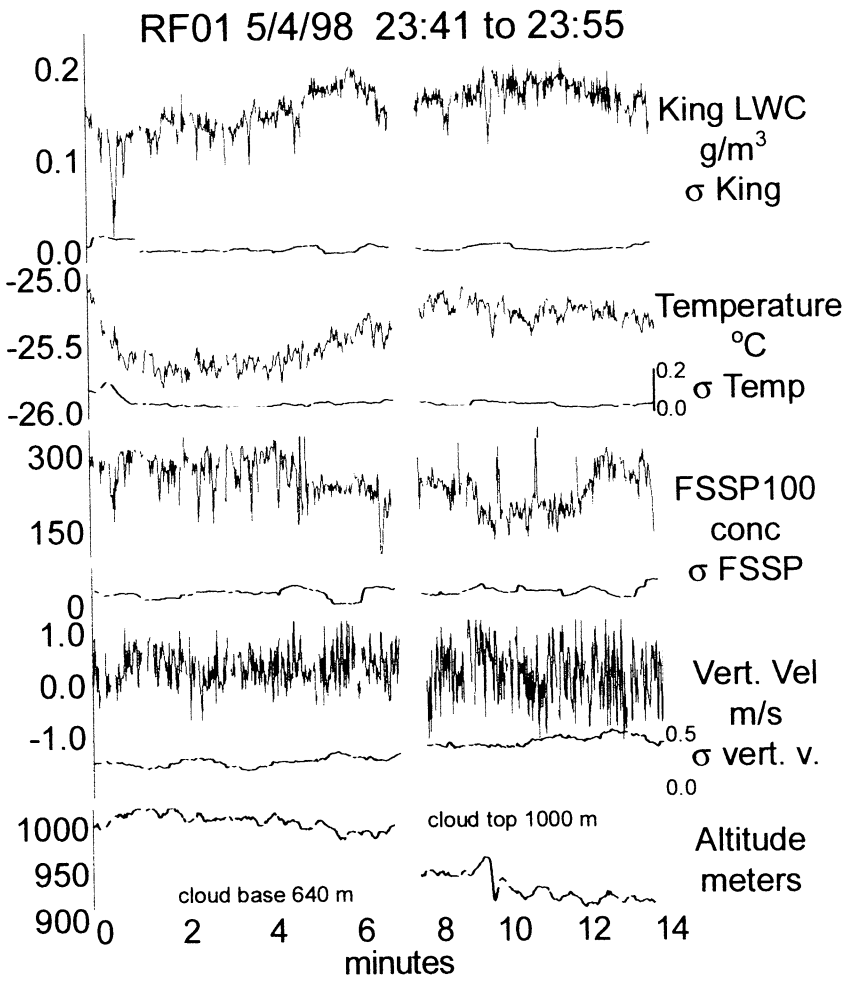

Figure 12. Time series of measurements and their standard deviations made by the C-130 as it flew different level passes through a boundary layer cloud on May 4, 1998.

paper. The cloud extended from about 2 km to 6 km msl (+2° to -23°C) on July 18, 1998 and contained a myriad of microphysical characteristics. Plate 2 shows a vertical profile of King LWC, FSSP, 260X, and 2D-C (shadow-or) particle concentration measurements, along with water and ice particle size distributions collected as the C-130 ascended from cloud base to cloud top. Representative examples of CPI images of the particles are also shown.

The data from the microphysical measurements shown in Plate 2 will be discussed from cloud top down to cloud base. In the upper portion of cloud, from cloud top at -23°C to -13°C, the FSSP droplet concentration varies from about 50 to 250 cm^{-3}, averaging about 125 cm^{-3}, and the LWC ranges from zero to 0.18 g m^{-3}, averaging about 0.1 g m^{-3}. The CPI drop size distribution shown in Plate 2 are relatively constant in this region but not especially broad, with 20 μm drops found in concentrations >1 cm^{-3} only in the regions with LWC > ~0.1 g m^{-3}. However, CPI images show a relatively low concentration of drizzle drops up to 125 μm in diameter near -19°C. The 260X measured a maximum of ~40 L^{-1} and the 2D-C shadow-or registered a maximum of 1 L^{-1}. This appears to be an example of "nonclassical freezing drizzle" formation [*Cober et al.*, 1996; *Lawson et al.*, 1998], where drizzle is formed through coalescence of supercooled drops, usually near the tops of stratus layers. However, in the Cober et al. and Lawson et al. measurements the FSSP drop spectra were generally broader and the 2D-C concentrations were significantly higher, in excess of 500 L^{-1}.

The CPI images show that ice particles were very rare in the region from -23°C to -13°C and were mostly large (750 μm) heavily rimed particles. The average 2D-C and 2D-P shadow-or particle concentrations are < 0.1 L^{-1} and support the observation that there was negligible ice in the layer. The lack of ice in the region from -23°C to -13°C is a curious aspect of this deep stratus cloud, because as will be shown, ice concentrations in the warmer regions below were much higher.

Near -12°C there is a noticeable drop in LWC to about <~0.01 g m^{-3}, a reduction in FSSP total particle concentration to about 5 cm^{-3} and a corresponding peak in 260X and 2D-C shadow-or concentrations. Plate 2 shows CPI images of some examples of the crystals, and Table 3 gives a breakdown of a visual classification of the particles. Plate 2 and Table 3 show that there is a mixture of crystal types, with about 65% of the number concentration composed of small (< 50 μm) spheroidal ice particles. Here spheroidal refers to image shapes that are not spherical (i.e., perfectly round) but instead have a slight but noticeable departure from a perfectly spherical shape. The remainder of the crystal types are mostly irregular shapes with a very small percentage (3%) of needles, sheaths,

Table 3. Classification of CPI Images From the Region With High Ice Concentration near -12°C on July 18, 1998

Category	Percentage	Rimed	Side Plane Growth
Spheroids	65%		
Needles, sheaths, columns	2%	1%	
Heavily rimed particles, graupel	1%	1%	
Irregular	32%	7%	14%
Total	100%	9%	14%

A total of 199 particles that were in very sharp focus were classified. All numbers shown are a percentage of total particles.

columns, graupel and aggregates. Only 9% of the crystals were rimed and 14% had side plane growth.

The CPI particle size distributions in Plate 2 show that ice existed in concentrations of about 2500 L^{-1} in the region around -12°C. Plate 3 shows the FSSP/CPI/260X combined particle size distribution in the "central" region with high ice concentrations, and in an "adjacent" region (i.e., the region encountered just prior to sampling the central region), where the ice concentration is reduced to about 750 L^{-1} and the FSSP concentration increases to about 100 cm^{-3}.

The microphysical data in Plates 2, 3, and Table 3 indicate that the (central) region of high ice concentration is composed of ice particles whose population is dominated by small (< 50 μm) ice spheroids that are not round but cannot also be identified as vapor-grown crystals. They could be frozen drops, or drops that were once frozen to larger ice particles, or even fragments of larger ice particles. The larger ice particles are mostly irregular in shape and sometimes contain side plane growth. In the "adjacent" regions immediately outside of the area with high ice particle concentrations the FSSP water drop concentration is much higher (up to 100 cm^{-3} compared to 5 cm^{-3}). The most striking feature in the "adjacent" regions is that there are more large, heavily rimed crystals, much more of the overall population of crystals is rimed and there are fewer small spheroids compared to the "central" region.

In the region from about -11°C to -7°C the LWC fluctuates between zero and 0.05 g m^{-3}, and the FSSP droplet concentration ranges from 50 to 100 cm^{-3}. CPI images show relatively low concentrations of rimed ice particles up to 500 μm and occasional drizzle drops in excess of 100 μm. The activity on the 260X and 2D-C are also relatively low, indicating few particles larger than 40 to 50 μm.

Very high concentrations (~4000 L^{-1}) of ice particles were also observed in the region from about -3.3°C to -5.5°C. This is a region that is often associated with the Hallett-Mossop (H-M) rime-splintering ice multiplication process. The conditions for H-M ice multiplication are [*Hallett and Mossop*, 1974; *Mossop and Hallet*, 1974; *Mossop*, 1985) as follows (1) cloud temperatures between -2.5° and -8°C, (2) droplets ≥ 23 μm in concentrations > 1 cm^{-3}, and (3) relatively fast falling (>0.2 to 5 m s^{-1}) ice particles.

The FSSP total particle concentration ranges from 2 to 20 cm^{-3} and averages about 5 cm^{-3} in the region with high ice concentration near -4.5°C. Plate 4 shows particle size distributions and CPI images in a format similar to that shown in Plate 3, and Table 4 shows a classification of ice particles in a format like Table 3. Again, like the region near -12°C, about two-thirds of the ice particles are small spheroids. The percentage of irregulars decreased from 32% to 14%. There are lower percentages of crystals with riming and side plane growth and the percentage of vapor grown crystals is 12%, compared to 2% at -12°C. The conditions for H-M ice multiplication are met in the central region if one assumes that the FSSP is only responding to water drops. However, as shown from the CPI data in Table 4 and Plate 4, the large majority if not all of the particles with sizes greater than about 25 μm are actually ice, so that the H-M criteria for drops > 23 μm in concentrations exceeding 1 cm^{-3} is not actually satisfied in the central region. Furthermore, the Rosemount icing detector did not register any supercooled water in the regions with high ice particle concentrations at -12°C and -4.5°C, which strongly suggests that these regions were nearly or entirely glaciated. *Mazin et al.* [2000] have shown that the theoretical sensitivity of the Rosemount icing detector is about 0.005 g m^{-3} under these thermodynamic conditions, so supercooled liquid water in excess of this threshold would be observed by the probe. The King probe (Plate 2) does indicate a small amount (0.02 to 0.05 g m^{-3}) of liquid water. This is explained as a "false LWC signal" due to ice particles

Table 4. Classification of CPI Images From the Region With High Ice Concentration near -4.5°C on July 18, 1998

Category	Percentage	Rimed	Side Plane Growth	Aggregates
Spheroids	71%			
Needles, sheaths, columns	9%			1%
Short columns, thick plates	3%			
Heavily rimed particles, graupel	3%	3%		
Irregular	14%	3%	1%	
Total	100%	6%	1%	1%

A total of 554 particles that were in very sharp focus were classified. All numbers shown are a percentage of total particles.

striking and melting on the wire. *Cober et al.* [2000] have shown that under these thermodynamic conditions, hot-wire probes will register a false LWC signal that is about 15 to 20% of the equivalent ice mass content.

The H-M conditions do appear to be satisfied in the regions adjacent to the central region with high concentrations near -4.5°C. The ice concentrations in these regions are still above those expected from primary nucleation but are about 25% of the ice concentration in the central region.

The mechanism(s) that is producing the very high ice particle concentrations in the regions near -12°C and -4°C is not obvious. *Rangno and Hobbs* [this issue] (hereinafter referred to as R-H) also report ice concentrations in a FIRE ACE stratus cloud that exceed those expected from primary nucleation, such as the ice nuclei concentrations collected in FIRE ACE by *Rogers et al.* [this issue]. However, R-H did not use CPI data to separate the contributions of water drops and ice and then to measure the total ice particle concentration. Instead, they used 2D-C measurements to determine the total ice particle concentration, which from Plate 2 can be seen to be a conservative (i.e., underestimate) of the actual concentration of ice, because particles <50 μm are rarely detected. R-H did use CPI data to visually classify the types of ice particles in a format similar to Tables 3 and 4. While this type of manual classification is somewhat subjective, it is interesting to note that both analyses reveal a very high concentration of small ice spheroids (which R-H labeled frozen drops) and particles that were fragments or irregular shapes. The percentage of frozen drops, fragments, and irregulars from the R-H analysis totaled 57% of the total ice particle population, and in this study, they totaled 97% and 85% in the regions near -12°C and -4°C, respectively. R-H point out that if the high ice concentrations were due to the H-M ice multiplication mechanism, the H-M small splinters would grow by vapor diffusion into crystals with identifiable habits, and in their case and here, this does not appear to be the dominate process. R-H also discuss in detail other possible ice multiplication mechanisms involving shattering of isolated drops during freezing and fragmentation of ice crystals by collisions. They conclude that either mechanism may have been operating but seemed to slightly favor the fragmentation process, since it appeared to better fit the observations.

Nearly all of the larger ice particles in the "adjacent" regions are heavily rimed. As seen in Plates 3 and 4, individual drops which could be susceptible to breaking off are frozen onto these large particles. It is also interesting to note that the small spheroids in the 'central' regions look as if they could be fragments that have broken from the large rimed crystals. There is no established physical mechanism to support this hypothesis, however, a similar process of rime breakup has been suggested by *Vali* [1980].

There is a thin layer of supercooled cloud from -2°C to about 0°C which has the highest (0.22 g m^{-3}) LWC and the highest (280 cm^{-3}) FSSP droplet concentration observed anywhere in the cloud. Also, the CPI detected no ice particles in this region and the 260X and 2D-C shadow-or concentrations were near zero, suggesting that this was a cloud composed of small water drops. It is difficult to explain why the large particles observed above in the cloud are not seen falling through this region of supercooled cloud. This is especially difficult to explain because drizzle was observed below the freezing level, presumably the result of melting of the larger ice particles. However, since the C-130 is climbing at a shallow angle, so that the data shown in Plate 2 do not actually comprise a vertical profile, it is possible that extreme variability in horizontal structure in the cloud (such as seen in Plate 1) can explain this observation.

6. Cirrus Cloud With High Concentrations of Small Ice Particles and Inhomogeneous Particle Distribution

Here we focus on the relatively high concentrations of small ice particles and the extreme spatial variability ("clumpiness") of ice particles seen in a cirrus cloud. Figure 13

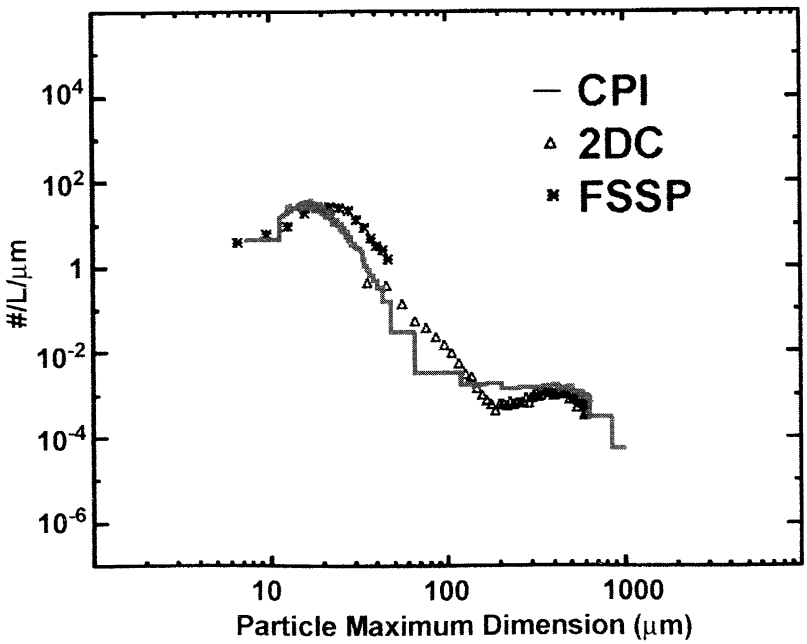

Figure 13. Particle size distributions measured by the FSSP (asterisks), CPI (solid line), and the 260X (triangles) for an Arctic cirrus cloud observed on July 29, 1998.

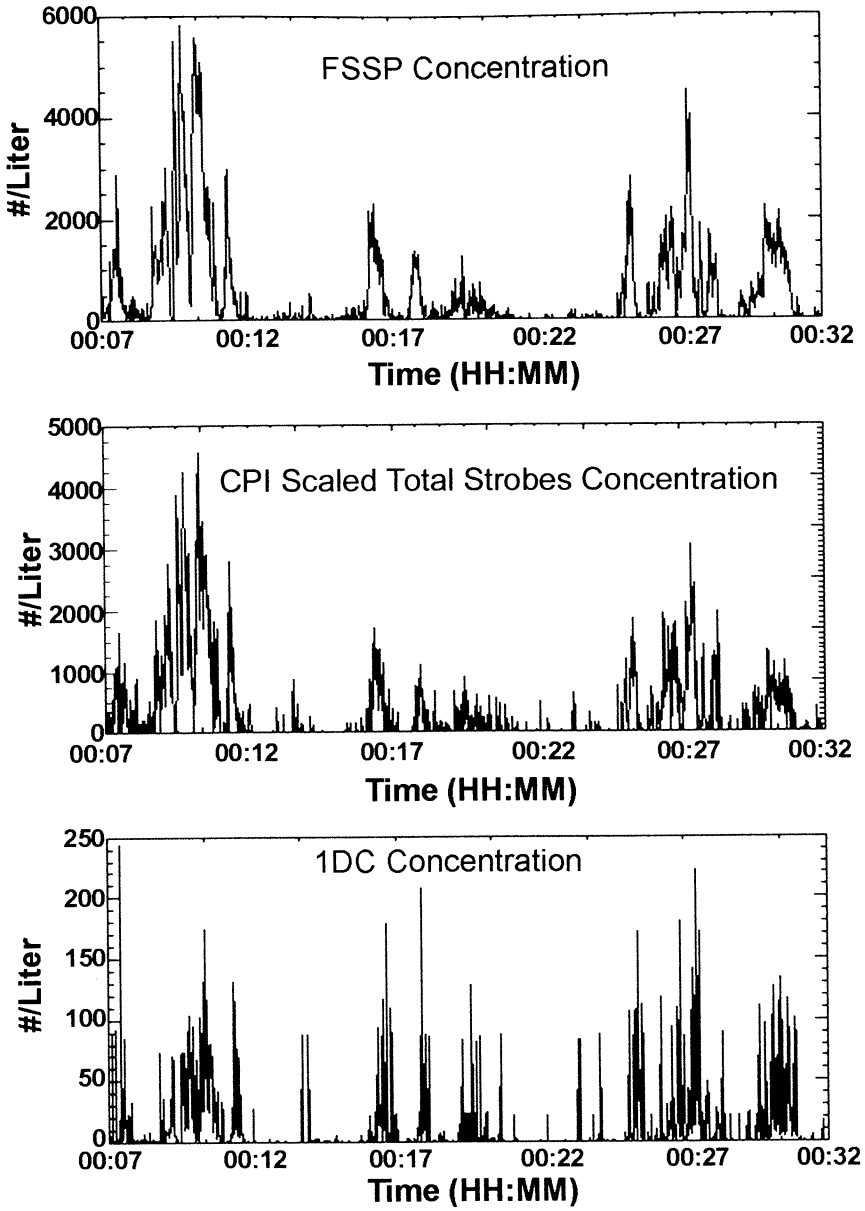

Figure 14. Time series of particle concentrations measured by various instruments while passing through an Arctic cirrus cloud on July 29, 1998 (the time shown is actually July 30, 1998, starting at 0007 UTC).

shows a combined particle size distribution using FSSP, CPI, and 260X data as the aircraft flew through cirrus clouds at 5400 m (-25°C) for approximately 25 minutes on July 29 1998. The Rosemount icing detector showed that there was no supercooled liquid water present in this cloud, so all of the particles are assumed to be of ice. The CPI particle size distribution was scaled to the 260X data in the 150 to 500 μm size region, where the 260X measurements are felt to be most reliable. The three particle size distributions show relatively good agreement in the regions where they overlap. A time series of average concentrations measured by the FSSP, CPI, and 260X are shown in Figure 14. In Figure 14, the CPI "scaled total strobes" particle concentration measurements have been scaled to the total particle concentration from the CPI size distribution in Figure 13. The time series show that the FSSP and CPI measure particle concentrations in the range of 1000 L^{-1} to 5000 L^{-1} over a 20 km region. The measurements also show that there is considerable spatial structure to the cloud on scales greater than the 120 m resolution of the instruments.

The FSSP is considered here to be a reliable measurement of the average concentration of small particles in cirrus clouds. Previous reports in the literature [e.g., *Gardiner and Hallett*, 1985] suggest that the FSSP is unreliable in the presence of ice. However, these measurements were in mixed-phase clouds where contributions from ice particles and water drops were difficult to separate. More recently, the literature contains FSSP measurements that are felt to be mostly reliable when the probe is measuring small ice particles in cirrus [e.g., *Gayet et al.*, 1996; *Poellot et al.*, 1999; *Arnott et al.*, 2000). The reasoning for using the FSSP data as a measure of average ice particle concentration in

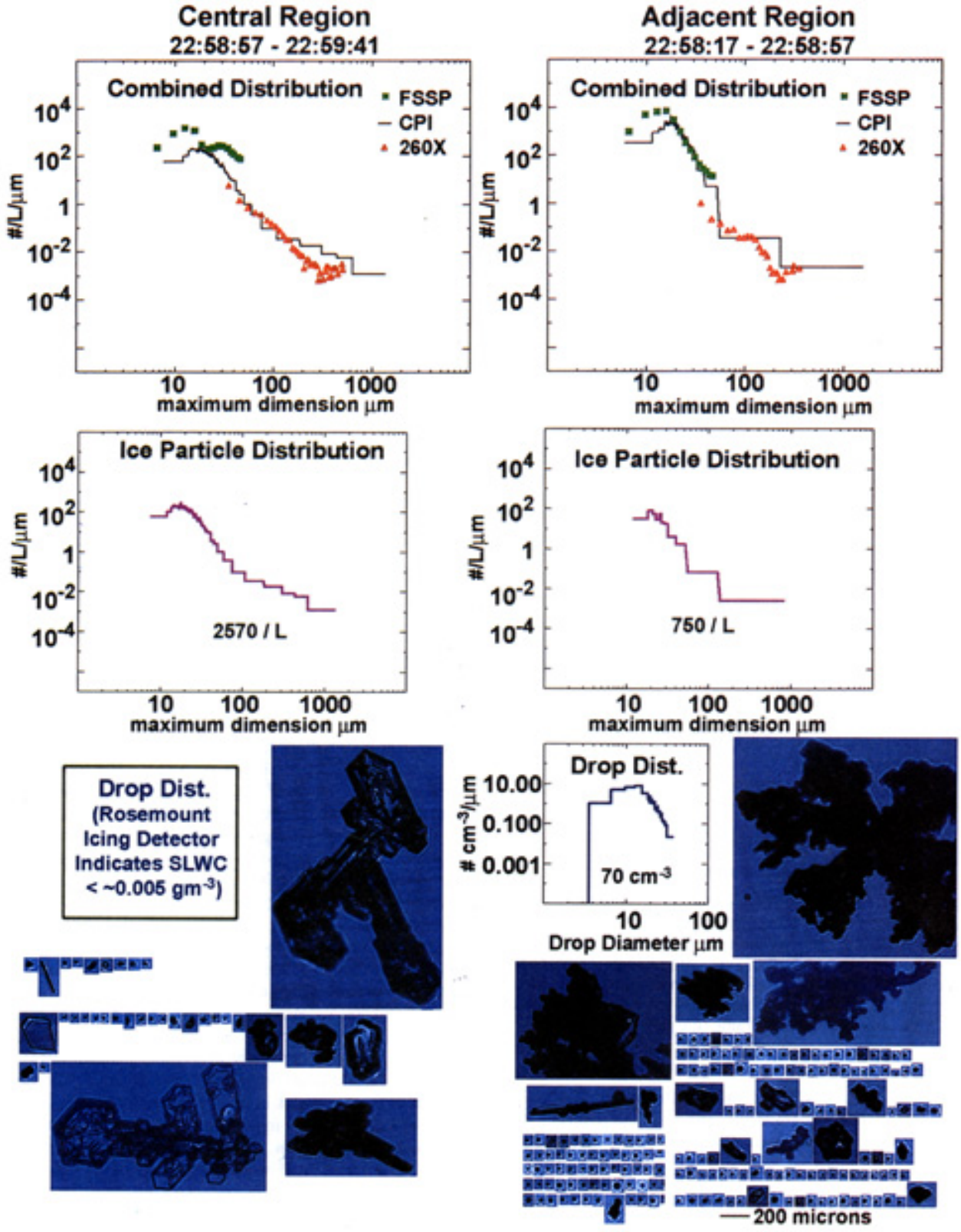

Plate 3. Total particle size distributions measured by the FSSP (asterisks), CPI (solid line), and 260X (triangles) in the "central" region with high ice concentrations near –12°C and the "adjacent" regions immediately above and below the central region. Water and ice particle size distributions are derived from CPI image data; examples of CPI images are also shown.

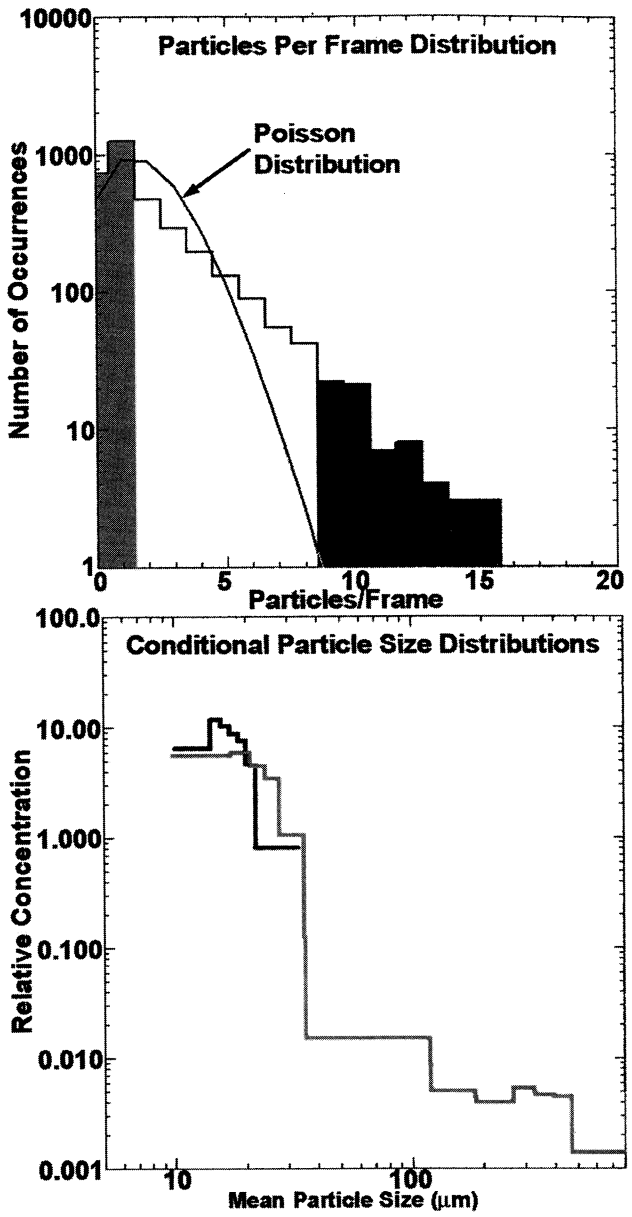

Figure 15. (top) Histograms of the number of particles per frame for all the CPI-imaged frames during the time period shown in Figure 14 along with the Poisson distribution with the same mean, and (bottom) conditional particle size distributions produced by using only those particles in frames with nine or more particles (black) and by using only particles that were imaged alone in a frame (grey).

cirrus is as follows: (1) CPI imagery shows that small (< 40 μm) particles in cirrus are largely spheroidal in shape, so even though the probe may not size these particles as accurately as it does water drops, it will still record a signal from the forward diffraction peak that will be registered as a count. (2) The FSSP-100 has a 6 μs dead time, so particles traveling at the (~120 m s^{-1}) airspeed of the C-130 in cirrus must be > ~750 μm to produce a double count. In addition, Figure 13 shows that the number of particles larger than 750 μm is four orders of magnitude less than the contribution of the smaller particles, so even if there were double counts from the large particles, they would have a negligible contribution.

The time series measurements from the FSSP, CPI, and 260X agree very well in phase (i.e., the peaks and valleys line up well). The concentrations measured by the FSSP are about 30% greater than those measured by the CPI, and both the FSSP and the CPI are more than an order of magnitude greater than the 260X concentrations. This is largely because, as shown in Figure 13, both the FSSP and the CPI data show large numbers of small particles, and high concentrations of small particles are more effectively counted by the FSSP and the CPI. The first useable channel in the 260X started at 40 μm, compared to 3 μm for the FSSP, while the smallest resolvable CPI image is about 10 μm. The ice particle concentrations shown here are nearly an order of magnitude greater than commonly found in cirrus literature (e.g., Heymsfield and Platt, 1984; Dowling and Radke, 1990). This is explainable because previous investigations did not include FSSP measurements and used only the 2D-C probe, which is known to miss the large majority of particles <50 μm in diameter. Relatively high ice particle concentrations are not found in Arctic cirrus. *Schmitt et al.* [2000] and *Baker et al.* [2000] also show FSSP and CPI measurements of high ice particle concentrations in mid-latitude cirrus.

We now return to the discussion of the highly inhomogeneous particle distribution, or "clumpiness," in this cirrus cloud, which is independent of the absolute magnitudes of the average particle concentrations shown in Figure 14. Figure 15 (top) shows the distribution of the number of particles per CPI image frame and the Poisson distribution with the same mean. As explained in the text describing Figure 3, the Poisson distribution would be the result of random sampling in a homogeneous cloud; the comparison in Figure 15 (top) shows that the cloud is inhomogeneous.

We now show that small particles are found in clumps with very high local concentrations that are interspersed with regions of larger particles in low concentrations. The conditional size distributions (analogous to Figure 3 (bottom) and 11 (bottom)) are shown in 15 (bottom). One conditional distribution was made of the sizes of particles imaged in frames with only one particle, while the other was made from the sizes of particles imaged in frames with seven or more particles. If the cloud were homogeneous, the conditional size distributions would be identical. However, as seen in Figure 15 (bottom), the high concentration frames contain only small particles; that is, the large particles are most often found in concentrations so low that to capture more than one particle in a frame is rare. When there are more than five particles in an image frame, the local concentration is on the order of 100,000 L^{-1} and higher. The small particles can be found at low concentration and at extremely high concentration. The conditional size distributions shown in Figure 15 (bottom) could result from the aircraft flying first through a region of large particles in low concentration, followed by a region of small particles in high concentrations, similar to the large-scale structure that caused the conditional spectra to separate in Figure 11. However, inspection of the CPI image frames themselves, shown in Plate 5, reveals that the regions of high concentrations of small particles are interspersed with regions of low concentrations of large particles, mostly bullet rosettes, on scales down to tens of meters and perhaps smaller. *Baker et al.* [2000] also observed regions with clumps of small particles separated by regions with single rosettes and aggregates of rosettes in a midlatitude cirrus cloud.

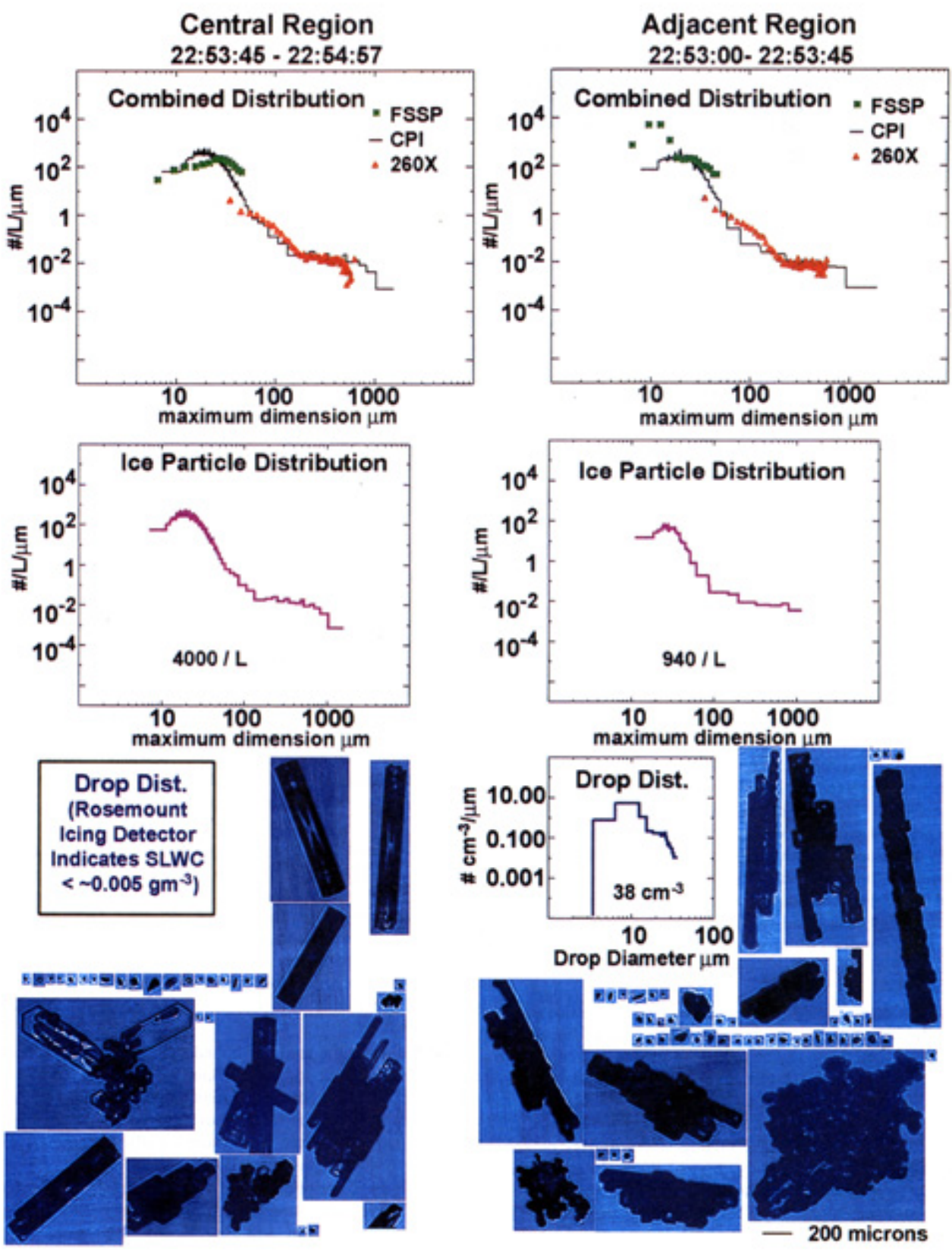

Plate 4. As in Plate 3, except for the "central" and "adjacent" regions near −4.5°C.

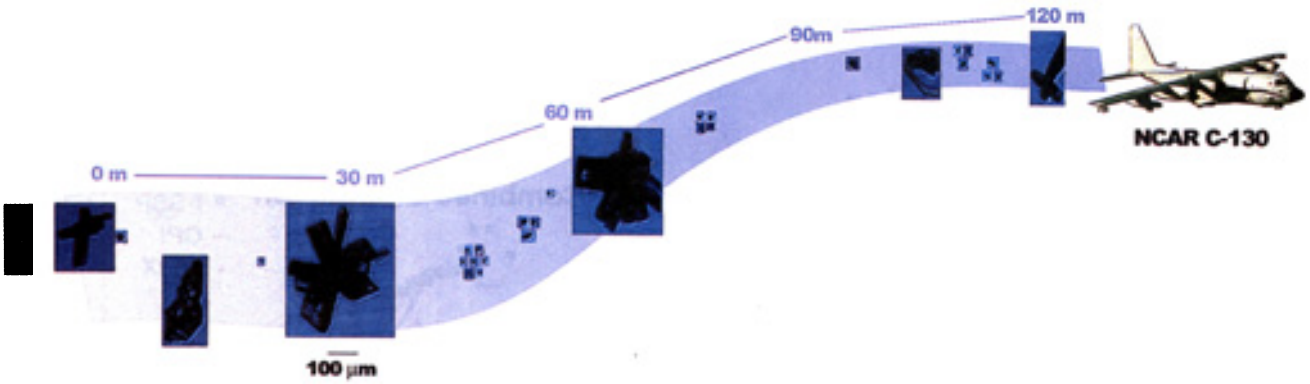

Plate 5. Images of Arctic cirrus ice particles sampled on July 29, 1998, during FIRE ACE. Each box with a large crystal and each group of small boxes represents one CPI image frame. The image frames reflect the relative positions of the particles along the flight track. A significant point here is that the spatial variation between low concentrations of large particles and high concentrations of small particles.

7. Summary

This research investigated microphysical data collected by the NCAR C-130 during the FIRE ACE field experiment conducted over the Beaufort Sea in May and July 1998. The standard microphysical measurements in the NCAR C-130 were supplemented, for the first time, with data collected by the Cloud Particle Imager (CPI). CPI data were used to separate spherical images (i.e., water drops) from non-spherical images (ice particles) in mixed-phase clouds. The CPI images also provide a method for determining inhomogeneity in the cloud particle field. CPI data were combined with conventional PMS FSSP and 260X particle data to determine total particle concentration, and the phase-discriminating capability of the CPI was used to determine the water and ice particle size distributions.

A major focus of this investigation concentrated on the microphysical properties of Arctic boundary layer clouds, which were observed on 11 of the total of 16 missions flown by the C-130. Here we define boundary layer clouds in the sense previously described by *Curry et al.* [1988], where the clouds are essentially low-lying stratus clouds that may or may not be thermodynamically connected with the surface. These boundary layer clouds were found to vary considerably, both from day to day and within the clouds themselves. The main microphysical features of the boundary layer clouds, based on data collected by the C-130, can summarized as follows:

1. From data collected during the 16 aircraft missions and the definition used here to define the presence of boundary layer cloud (i.e., thermally mixed to the surface and/or within 300 m of the surface), 11 of the 16 days had boundary layer clouds. In May, six out of eight cases had boundary layer clouds, and all six clouds were mixed from the surface to cloud base. The depths of the mixing layers in May ranged from 150 to 1200 m. In July, five of the eight cases had boundary layer clouds, but none of these were mixed from the surface to cloud base. Thus based on these (limited) data, low-lying clouds in the Arctic, which have been shown to strongly influence the melt of the Arctic Ocean ice pack [*Curry et al.*, 1993], were prevalent and displayed significantly different subcloud mixing characteristics in May and July.

2. On the basis of analysis of data from 21 vertical (slant) profiles flown on 4 days in essentially all-water clouds, nine of the profiles revealed mostly homogeneous, adiabatic conditions with monomodal drop size distributions and no drizzle drops. Data from the remaining 12 profiles indicate that these clouds were either too thin to have adequate LWC to determine whether they were adiabatic or that they were actively mixing from cloud top downward. In the latter cases the LWC and temperature in the upper portion of cloud were generally nonadiabatic, and the clouds were inhomogeneous. The drop size distributions were often bimodal near cloud top, and drizzle was sometimes observed.

3. The adiabatic regions of clouds were used to evaluate the performance of the LWC probes, although the adiabatic LWC never exceeded 0.4 g m^{-3} in these thin clouds, so the instruments were only evaluated within a relatively low range of LWC. The two King probes generally did not exceed the adiabatic value and were within 75% of adiabatic. The Gerber PVM probe scattered around the adiabatic value and sometimes exceeded it by up to about 35%. The FSSP systematically exceeded the adiabatic LWC value by up to a factor of 2.

4. A mixed-phase boundary layer cloud investigated on May 4, 1998 that was 360 m thick and ranged in temperature from -22° to -25°C displayed considerable variation in hydrometeor fields. On the basis of CPI measurements, regions about 10 km across and separated by only 100 m in the vertical contained either small cloud drops and few ice particles, drizzle or graupel particles. Seeding from cirrus clouds aloft probably influenced the microphysical processes in this cloud.

In addition to the study of boundary layer clouds, a deep stratus cloud with cloud base at 2 km (+2°C) and cloud top at 6 km (-23°C) was studied. Examination of the microphysics in this deep stratus cloud revealed extreme variability in cloud particles and two layers with exceptionally high (2500 to 4000 L^{-1}) concentrations of small ice particles.

Starting the description of the stratus cloud from the top down, a region of supercooled drizzle (at -19°C) was observed near cloud top, and supercooled cloud drops with very low (~0.1 L^{-1}) ice concentrations were observed from cloud top to the -13°C level. In a thin layer around -12°C, very high (~ 2500 L^{-1}) ice concentrations were observed, with about 97% of the ice identified as small (< ~ 50 µm) spheroidal (but not perfectly round) particles, fragments and irregular shapes. Only 2% of the ice appeared to be vapor

grown. Relatively low ice concentrations and small amounts of supercooled liquid water were observed between -11°C and -7°C. From -5.5°C to -3.3°C, another layer with very high (4000 L^{-1}) ice particle concentrations was observed. Although this layer was within the temperature regime where the Hallett-Mossop ice multiplication process is often observed, there were insufficient drops > 23 μm to meet the Hallett-Mossop criteria. Instead, the FSSP appeared to be responding to the small ice spheroids observed by the CPI, since the Rosemount icing detector did not measure any supercooled liquid water. The ice particles in this region were similar to those observed at -12°C, with the main difference being less (85%) small spheroids and more vapor grown crystals. *Rangno and Hobbs* [this issue] analyzed CPI images from another FIRE ACE stratus cloud and found that 57% of the ice particles were "frozen drops" (presumably similar to our small spheroids), fragments, and particles with irregular shapes. Rime breakup, fragmentation from crystal collision, and drop shattering are discussed as possible ice multiplication mechanisms, but there is no physical way to adequately verify any of these processes. Drizzle was observed precipitating through cloud base of this deep stratus cloud.

An Arctic cirrus cloud was also investigated and shown to be highly inhomogeneous on scales down to tens of meters or less. Regions with high concentrations of small ice particles are interspersed with regions of low concentrations of large particles, mostly bullet rosettes. The CPI images showed that the regions with small ice particles were in very high (~100,000 L^{-1}) local concentrations. The FSSP and CPI probes measured a 20 km average cirrus particle concentration that ranged from about 1000 L^{-1} to 5000 L^{-1}, which is considerably higher than previously reported in the literature.

The variability in the microphysical properties of Arctic stratus (boundary layer, deep stratus, and cirrus) clouds, both within a cloud and from cloud to cloud, presents a challenge for Arctic column and process modelers alike. The variability of hydrometeor types and concentrations within Arctic stratus clouds also presents a challenge to investigators retrieving microphysical properties from remote measurements. While presenting these challenges, Arctic stratus clouds also offer the benefit of being relatively easy to study with large turboprop and jet aircraft in the summer months, in that they are persistent and cover extensive areas.

Acknowledgments. We would like to thank Judith Curry at the University of Colorado for her direction of the scientific research and her insightful comments on this manuscript. Kim Weaver and Pat Zmarzly of SPEC provided superb engineering support of the CPI. The staff at the NASA FIRE Project Office provided excellent logistical support. We are also indebted to the NCAR Research Aviation Staff for their scientific and instrumentation support, and to the crew of the C-130 for their skillful piloting and maintenance of the aircraft. Finally, we are grateful to Margaret Hogue at the AGU publications office for her valuable assistance and patience. This work has been funded under the NASA FIRE program, contract NAS1-96015 and NSF Grant ATM-9904710.

References

Arnott, P. A., D. Mitchell, C. G. Schmitt, D. Kingsmill, and D. Ivanova, Analysis of the FSSP performance for measurements of small crystal spectra in cirrus, paper presented at 13th International Conference on Clouds and Precipitation, International Commission on Clouds and Precipitation, Reno, Nev., August 14 - 18, 2000.

Baker, B. A., R. P. Lawson, and C. G. Schmitt, Clumpy cirrus, paper presented at 13th International Conference on Clouds and Precipitation, International Commission on Clouds and Precipitation, Reno, Nev., August 14 - 18, 2000.

Baumgardner, D., An analysis and comparison of five water droplet measuring instruments, *J. Appl. Meteorol., 22*, 891-910, 1983.

Baumgardner, D., Corrections for the response times of particle measuring probes, in Proceedings of *Sixth Symposium for Meteorological Observations and Instruments*, pp. 148-151, Am. Meteorol. Soc., Boston, Mass., 1987.

Baumgardner, D., and M. Spowart, Evaluation of the forward scattering spectrometer probe, part III, Time response and laser inhomogeneity limitations, *J. Atmos. Oceanic Technol., 7*, 666-672, 1990.

Baumgardner, D., W. Strapp, and J. E. Dye, Evaluation of the forward scattering spectrometer probe, part II, Corrections for coincidence and dead-time losses, *J. Atmos. Oceanic Technol., 2*, 626-632, 1985.

Baumgardner, D., W. A. Cooper, and J. E. Dye, Optical and electronic limitations of the forward-scattering spectrometer probe, in *Limited Particle Size Measurements Techniques,* 2nd vol., *ASTM STP, 1083,* 115-127, 1990.

Biter, C. J., J. E. Dye, D. Huffman, and W.D. King, The drop-size response of the CSIRO liquid water content probe, *J. Atmos. Oceanic Technol., 4*, 359-367, 1987.

Brenguier, J.-L., Coincidence and dead-time corrections for particle counters, part II, High concentration measurements with an FSSP, *J. Atmos. Oceanic Technol., 6*, 585-598, 1989.

Cerni, T. A., Determination of the size and concentration of cloud drops with an FSSP, *J. Clim. Appl. Meteorol., 22*, 1346-1355, 1983.

Cober, S.G., J.W. Strapp, and G.A. Isaac, An example of supercooled drizzle drops formed through a collision-coalescence process., *J. Appl. Meteorol., 35*, 2250-2260. 1996.

Cober, S.G., G.A. Isaac, Korolev, A. V., and J. W. Strapp, Assessing the relative contributions of liquid and ice phases in winter clouds, paper presented at 13th International Conference on Clouds and Precipitation, International Commission on Clouds and Precipitation, Reno, Nev., August 14 - 18, 2000.

Cooper, W. A., Effects of coincidence on measurements with a forward scattering spectrometer probe, *J. Oceanic Atmos. Technol., 5*, 823-832, 1988.

Curry, J.A., Interactions among turbulence, Radiation and microphysics in Arctic stratus clouds, *J. Atmos. Sci., 43*, 90-106, 1986.

Curry, J. A., E. E. Ebert, and G. F. Herman, Mean and turbulence structure of the summertime Arctic cloudy boundary layer, *Q. J. R. Meteorol. Soc., 114*, 715-746, 1988.

Curry, J.A., F.G. Meyer, L.F. Radke, C.A. Brock, and E.E. Ebert, Occurrence and characteristics of lower tropospheric ice crystal in the Arctic, *Int. J. Climatol., 10*, 749-764, 1990.

Curry, J.A., E.E. Ebert, and J.L. Schramm, Impact of clouds on the surface radiation balance of the Arctic Ocean, *Meteorol. Atmos. Phys., 51*, 197-217, 1993.

Curry, J.A., W.B. Rossow, D.A. Randall, and J.L. Schramm, Overview of Arctic cloud and radiation characteristics, *J. Clim., 9*, 1731-1764, 1996.

Curry, J.A., J.O. Pinto, T. Benner, and M. Tschudi, Evolution of the cloud boundary layer during the autumnal freezing of the Beaufort Sea, *J. Geophys. Res., 102,* 13,851-13,860, 1997.

Curry, J.A., et al., FIRE Arctic Clouds Experiment, *Bull. Am. Meteorol. Soc., 81*, 5-29, 2000.

Dowling, D. R., and Radke, L. F., 1990. A summary of the physical properties of Cirrus clouds., *J. Appl. Meteor., 29*, 970-978.

Dye, J.E., and D. Baumgardner, Evaluation of the forward scattering spectrometer probe, part I, Electronic and optical studies, *J. Atmos. Oceanic Technol., 1*, 329-344, 1984.

Gardiner, B.A., and J. Hallett, Degradation of in-cloud forward scattering spectrometer probe measurements in the presence of ice crystals, *J. Atmos. Oceanic. Technol.*, 171-180, 1985.

Garrett, T., and P.V. Hobbs, Calibration of liquid water probes from the University of Washington's CV-580 aircraft at the Canadian NRC wind tunnel, in *Rep. Cloud and Aerosol Research Group*, 20 pp., Dep. of Atmos. Sci., Univ. of Washington, Seattle,1999.

Gayet, J., G. Febvre, and H. Larsen, The reliability of the PMS FSSP in the presence of small ice crystals, *J. Atmos. Oceanic Technol., 13*, 1300-1310, 1996.

Gerber, H., B.G. Arends, and A.S. Ackerman, New microphysics sensor for aircraft use, *Atmos. Res., 31*, 235-252, 1994.

Heymsfield, A. J., and C. M. R. Platt, 1984: A parameterization of the particle size spectrum of ice clouds in terms of the ambient temperature and the ice water content. *J. Atmos. Sci., 32*, 799-808.

Hallett, J., and S.C. Mossop, Production of secondary ice particles during the riming process, *Nature, 249*, 26-28. 1974.

Intergovernmental Panel on Climate Change (IPCC), *Climate Change: The IPCC Scientific Assessment*, edited by J.T. Houghton, G.J. Jenkins, and J.J. Ephramus, 365 pp., Cambridge Univ. Press, New York, 1990.

Jayaweera, K.O.L.F., and T. Ohtake, Concentration of ice crystals in Arctic stratus clouds, *J. Rech. Atmos., 7*, 199-207, 1973.

Jensen, J. B., P. H. Austin, M. B. Baker, and A. M. Blyth, Turbulent mixing, spectral evolution and dynamics in a warm cumulus cloud, *J. Atmos. Sci., 42*, 173-192, 1985.

Jiang, H., G. Feingold, W. R. Cotton, and P. G. Duynkerke, Large-eddy simulations of entrainment of cloud condensation nuclei into the Arctic boundary layer: May 18, 1998, FIRE/SHEBA Case Study, this issue.

King, W. D., D. A. Parkin, and R. J. Handsworth, A hot wire liquid water device having fully calculable response characteristics, *J. Appl. Meteorol., 17*, 1809-1813, 1978.

Knollenberg, R.G., Techniques for probing cloud microstructure, in *Clouds, Their Formation, Optical Properties, and Effects,* edited by P.V. Hobbs and A. Deepak, pp. 15-91, Academic, San Diego, Calif., 1981.

Korolev, A.V., J.W. Strapp, and G.A. Isaac, Evaluation of the accuracy of PMS optical array probes, *J. Atmos. Oceanic Technol., 15*, 708-720, 1998.

Korolev, A.V., G.A. Isaac, and J. Hallett, Ice particle habits in Arctic clouds, *Geophys. Res. Lett., 26, (9),* 1299-1302, 1999.

Laursen, K., Project documentation summary, in *Natl. Cent. For Atmos. Res., Surface Heat Budget of the Arctic Ocean, NCAR RAF Proj. No. 8-101*, 1998.

Lawson, R. P., Improved particle measurements in mixed phase clouds and implications on climate modeling, in *Proceedings of the WMO Workshop on Measurement of Cloud Properties for Forecasts of Weather, Air Quality and Climate*, pp. 139-158, World Meteorol. Organ., Geneva, Switzerland, 1997.

Lawson, R. P., and A. M. Blyth, A comparison of optical measurements of liquid water content and drop size distribution in adiabatic regions of Florida cumuli, *Atmos. Res., 47-48*, 671-690, 1998.

Lawson, R. P., and W. A. Cooper, Performance of some airborne thermometers in clouds, *J. Atmos. Oceanic Technol., 7*, 480-494, 1990.

Lawson, R. P., and R. H. Cormack, Theoretical design and preliminary tests of two new particle spectrometers for cloud microphysics research, *Atmos. Res., 35*, 315-348. 1995.

Lawson, R.P., and T.L. Jensen, Improved microphysical observations in mixed phase clouds, in *Proceedings of the Conference on Cloud Physics*, pp. 451-454, Am. Meteorol. Soc., Boston, Mass., 1998.

Lawson, R. P., A. V. Korolev, S. G. Cober, T. Huang, J. W. Strapp, and G.A. Isaac, Improved measurements of the drop size distribution of a freezing drizzle event, *Atmos. Res., 47-48*, 181-191, 1998.

Mazin, I. P., A. V. Korolev, A. Heymsfield, G. A. Isaac, and S. G. Cober, Thermodynamics of icing cylinder for measurements of liquid water content in supercooled clouds, *J. Atmos. Oceanic. Technol.*, in press, 2000.

Mossop, S. C., Secondary ice particle production during rime growth: The effect of drop size distribution and rimer velocity, *Q. J. R. Meteorol. Soc., 111*, 1113-1124, 1985.

Mossop, S. C., and J. Hallet, Ice crystal concentration in cumulus clouds: Influence of the drop spectrum, *Science, 186,* 632-633, 1974.

Perovich, D.K., et al., Year in ice gives climate insights, *EOS, Trans. AGU, 80(41)*, 484-486, 1999.

Pinto, J. O., J. A. Curry, and J. M. Intrieri, Cloud-aerosol interactions during autumn over the Beaufort Sea, *J. Geophys. Res.*, this issue.

Poellot, M.R., W.P. Arnott, and J. Hallett, In situ observations of contrail microphysics and implications for their radiative impact, *J. Geophys. Res., 104,* 12,077-12,084, 1999.

Pruppacher, H. R., and J. D. Klett, *Microphysics of Clouds and Precipitation,* 707 pp., D. Reidel, Norwell, Mass., 1978.

Rangno, A. L., and P. V. Hobbs, Ice particles in stratiform clouds in the Arctic and possible mechanisms for the production of high ice concentrations, *J. Geophys. Res.*, this issue.

Rogers, D. C., P. J. DeMott, and S. M. Kreidenweis, Airborne measurements of tropospheric ice nucleating aerosol particles in the Arctic spring, *J. Geophys. Res.*, this issue.

Schmitt, C. G., R. P. Lawson, Baker, B. A., In situ measurements of mid-latitude and tropical cirrus clouds, paper presented at 13th International Conference on Clouds and Precipitation, International Commission on Clouds and Precipitation, Reno, Nev., August 14 - 18, 2000.

Vali, G., Ice multiplication by rime breakup, in *Communications à la VIIIème Conference Internationale sur la Physique des Nuages*, Vol. 1, pp. 227-228, Clermont-Ferrand, France, 1980.

Wendisch, M. A., Quantitative comparison of ground-based FSSP and PVM measurements, *J. Atmos. Oceanic Technol., 15*, 887 – 900, 1998.

Wendisch, M., A. Keil, and A.V. Korolev, FSSP characterization with monodisperse water droplets, *J. Atmos. Oceanic Technol., 13, (6)*, 1152-1165, 1996.

Witte, H.J., Airborne observations of cloud particles and infrared flux density in the Arctic, MS thesis, 102 pp., Dep. of Atmos. Sci., Univ. of Washington, Seattle, 1968.

Yum, S. S., and J. G. Hudson, Vertical distributions of cloud condensation nuclei spectra over the springtime Arctic Ocean, *J. Geophys. Res.*, this issue.

B. A. Baker, R. P. Lawson, and C. G. Schmitt, SPEC Inc. 5401 Western Avenue, Suite B, Boulder, CO 80301. (brad@specinc.com; plawson@specinc.com; cschmitt@specinc.com)

T. L. Jensen, Silver Lining Enterprises, 710 City Park Ave. #C312, Fort Collins, CO 80521. (info@projectspecialist.com)

(Received January 7, 2000; revised September 27, 2000; accepted October 2, 2000.)